The Journal of Chemical Physics PERSPECTIVE scitation.org/journal/jcp

Multidimensional electronic spectroscopy in high-definition—Combining spectral, temporal, and spatial resolutions

Cite as: J. Chem. Phys. 154, 230901 (2021); doi: 10.1063/5.0052234
Submitted: 30 March 2021 • Accepted: 20 May 2021 •
Published Online: 15 June 2021

Vivek Tiwari[a)]

AFFILIATIONS

Solid State and Structural Chemistry Unit, Indian Institute of Science, Bangalore, Karnataka 560012, India

Note: This paper is part of the JCP Special Topic on Coherent Multidimensional Spectroscopy.
[a)]**Author to whom correspondence should be addressed:** vivektiwari@iisc.ac.in

ABSTRACT

Over the past two decades, coherent multidimensional spectroscopies have been implemented across the terahertz, infrared, visible, and ultraviolet regions of the electromagnetic spectrum. A combination of coherent excitation of several resonances with few-cycle pulses, and spectral decongestion along multiple spectral dimensions, has enabled new insights into wide ranging molecular scale phenomena, such as energy and charge delocalization in natural and artificial light-harvesting systems, hydrogen bonding dynamics in monolayers, and strong light–matter couplings in Fabry–Pérot cavities. However, measurements on ensembles have implied signal averaging over relevant details, such as morphological and energetic inhomogeneity, which are not rephased by the Fourier transform. Recent extension of these spectroscopies to provide diffraction-limited spatial resolution, while maintaining temporal and spectral information, has been exciting and has paved a way to address several challenging questions by going beyond ensemble averaging. The aim of this Perspective is to discuss the technological developments that have eventually enabled spatially resolved multidimensional electronic spectroscopies and highlight some of the very recent findings already made possible by introducing spatial resolution in a powerful spectroscopic tool.

I. INTRODUCTION

Electronic and vibrational motions are known to drive quantum relaxation processes on the fastest timescales.[1,2] Fundamental aspects of the above molecular scale physics, although occurring on femtosecond to picosecond timescales, may impact macroscopic phenomena, such as the nature of human vision,[3] photocurrent efficiency of photovoltaic devices,[4] and natural photosynthesis.[5] Typically, the above relaxation processes occur between several overlapping vibrational–electronic (vibronic) bands in condensed phase dissipative environments, rendering a purely experimental determination of the underlying relaxation mechanisms quite challenging.

In analogy with multidimensional nuclear magnetic resonance (NMR),[6,7] the advent of optical multidimensional spectroscopic techniques has partly addressed the above issue by spectrally decongesting relaxation processes in terms of a two-dimensional (2D) contour map, which correlates the excitation and detection frequencies of a system. Similar to spin echoes in NMR, Fourier transform multidimensional spectroscopy[8] can also rephase the ensemble dephasing of a collection of oscillating dipoles to reveal the homogenous dephasing timescale of an individual dipole in the ensemble. The 2D contour maps evolve with the pump–probe waiting time T and show the correlations between chromophores both within and across the vibronic bands excited by femtosecond pulses. However, multidimensional spectroscopies with single waiting times[9] do not rephase the energetic or morphological inhomogeneities in the sample along the pump–probe waiting time such that the underlying relaxation mechanisms between overlapping vibronic bands may still be obscured. These could be the timescales of homogeneous dephasing of coherences between excited states in an inhomogeneous distribution of energy gaps[10] or morphology dependence of singlet exciton fission[11] and exciton diffusion[12] rates.

The above limitations of multidimensional spectroscopy, which arise due to ensemble averaging of dynamics along T, are

connected to the fact that traditional experimental implementations[13] have relied on non-collinear or partly collinear geometries with the advantage of signal detection being completely or partially background-free, respectively. However, non-collinear phase-matching relies on having the volume of the amplitude and phase grating[14] imprinted by the pump pulses on the sample being much larger than the diffraction-limited volume imposed by the wavelength of light, thereby limiting the available spatial resolution. Sensitivity of detection of the radiated electric field from macroscopic polarization further constrains the possibility of sub-ensemble measurements. Recently, developments in acousto-optic phase-modulation and pulse shaping techniques[15,16] have paved the way for multidimensional electronic spectroscopy (MES) at the diffraction limit. This Perspective discusses the technological developments that have made this feasible and the new science already made possible by spatially resolved MES (srMES).

II. DEVELOPMENT OF COLLINEAR APPROACHES TO MULTIDIMENSIONAL ELECTRONIC SPECTROSCOPY

Several detailed reviews on the experimental and theoretical principles governing coherent multidimensional spectroscopy are available.[1,8,13] In order to understand the development of fully collinear approaches to MES and, therefore, the development of spatially resolved techniques, it is essential to discuss the experimental implementation aspects of typical multidimensional spectroscopic techniques, which are briefly summarized below.

A. Non-collinear geometry

A MES experiment is understood under the time-dependent perturbation framework where the combined effect of light–matter interactions initiated by incoming electric fields creates macroscopic polarization in the sample that oscillates at optical frequencies. Oscillating polarization radiates an electric field along directions where the wavevectors of the incoming electric fields interfere constructively. As shown in Fig. 1(a), in a typical experiment, three pulses are incident on the sample in a box*CARS* geometry, with wavevectors $\vec{k}_1$, $\vec{k}_2$, and $\vec{k}_3$ along three corners of a square. The signal electric field $\vec{E}_s$ is then radiated along the fourth corner of the square in a known, background-free, phase-matched direction. Interaction of the system with three incident pulses dominantly leads to a four-wave mixing process with the total three light–matter interactions from the input pulses. However, note that the total interaction of the system with three pulses also leads to more than three light–matter interactions, where contributions higher than third order may become significant. For instance, under high fluences or sample concentrations, fifth-order perturbative contributions[21] and third-order cascaded signals[22] can contribute along the same phase-matched direction. If not desirable, such contributions can be minimized[23] by controlling fluence, sample thickness, and concentration. Overall, the electric field radiated along the phase-matched direction is dominantly a frequency-domain product of

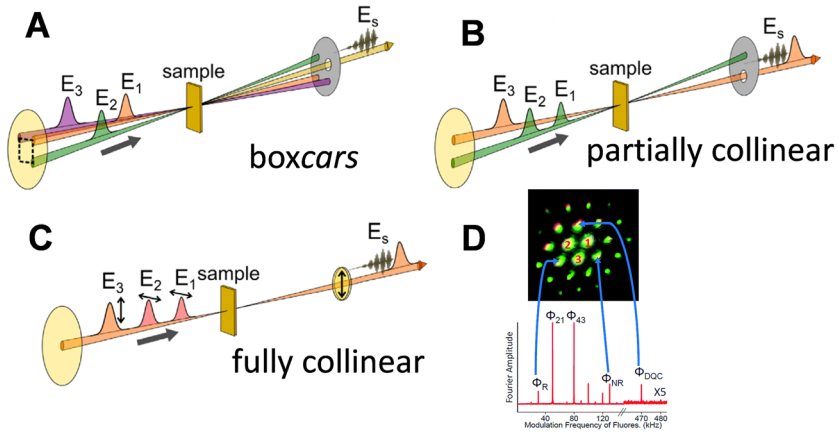

FIG. 1. Geometric considerations in multidimensional electronic spectroscopy (MES). (a) Traditionally, three unique wavevectors corresponding to electric fields $\vec{E}_1$, $\vec{E}_2$, and $\vec{E}_3$ are focused into the sample in a box-CARS geometry. The resulting signal $\vec{E}_s$ is radiated by macroscopic polarization in the sample along a background-free phase-matched direction, which results from a spatially coherent average over all the dipole oscillators within the illuminated area of the sample. This signal field is heterodyned with a known local oscillator (LO) field in order to fully reconstruct the phase and amplitude information in the signal field. (b) In a partly collinear pump–probe geometry, the wavevectors for $\vec{E}_1$ and $\vec{E}_2$ are degenerate such that the probe $\vec{E}_3$ acts as the local oscillator and $\vec{E}_s$ is not background-free. Additional signal filtering techniques are required to remove the probe background. (c) In the fully collinear geometry, all the wavevectors are degenerate and there is no phase-matched direction for $\vec{E}_s$. In order to filter the signal field, both the pump and probe backgrounds need to be filtered, ideally before photodetection. In addition to probe filtering techniques in the partly collinear geometry, pump filtering is typically achieved using spectral or polarization separation between the pump and probe beams. (d) An alternative approach to background filtering is the use of acousto-optic radio-frequency tagging of optical pulses. The resulting signal is a specific linear combination of input radio-frequency tags and is filtered using phase-sensitive lock-in detection.[17,18] Thus, each phase-matching direction, marked in blue, is now replaced with a particular combination of radio-frequencies. (a)–(c) are adapted with permission from C. R. Baiz, D. Schach, and A. Tokmakoff, Opt. Express **22**, 18724–18735 (2014). Copyright 2014 OSA. (d) is adapted with permission from Karki *et al.*, Chem. Sci. **10**, 7923–7928 (2019). Copyright 2019 the Royal Society of Chemistry.

the third-order material susceptibility with the three electric fields contributing to the light–matter interactions. This third-order signal is heterodyne-detected by interfering with a local oscillator (LO) field of a known phase, which is propagated along the same phase-matched direction as the signal field. Thus, a fully non-collinear phase-matched geometry has the advantage of background-free directional filtering of the signal. However, directional filtering is a consequence of spatially coherent average over the sample region that has been illuminated by the three input pulses and thus constrained by the extended sample volume over which a transient pump grating is imprinted. Note that in the case of semiconductor systems,[24] which are sensitive to excitation by the LO pulse focused on the sample, an additional reference beam that heterodynes the signal without transmitting through the sample is employed, at the cost of careful optical phase considerations between LO and reference fields. Since non-collinear geometry has a phase-matched direction along which a part of the probe pulse is diffracted by the pump-induced grating, integration of this geometry into a microscope objective is not only cumbersome geometrically but also will lead to a poor diffraction efficiency[14] from such a pump grating.

B. Collinear geometries

When a purely absorptive 2D electronic spectrum is desirable, different third-order non-linear responses need to be accurately phased and combined to result in a purely absorptive 2D line shape. However, phase and timing jitters in electronic spectroscopy can result in artificially twisted peak shapes due to jitter related mixing of absorptive and dispersive components. Gallagher Faeder and Jonas proposed[25] an easier experimental implementation for obtaining purely absorptive 2D spectra using a partially collinear pump–probe geometry compared to the box*CARS* geometry. As shown in Fig. 1(b), in this geometry, the two pump pulses are collinear, that is, the wavevectors of $\vec{k}_1$ and $\vec{k}_2$ are degenerate. Jonas and co-workers termed this easier implementation as homotime absorptive response detection, or HARD 2D, because now the probe field itself acts as the LO and homodynes with the signal. In the non-collinear geometry, the intensity of the LO field is tunable and allows for maximum fringe visibility between the signal and LO fields. Even though independent tunability of the probe is not possible in the partially collinear geometry, polarization and interferometric controls[13] can still allow for a probe background reduction, resulting in enhanced detection sensitivity.[26] Subsequent experimental implementations[13] in the partially collinear geometry have allowed[26] for a desirable separation of third-order non-linear response pathways while retaining the benefits of easier experimental implementation and phase stability of homodyne detection.

Implementation of MES in the partially collinear geometry already makes the possibility of integration with a microscope objective somewhat feasible. The time-delayed collinear pump pulses create an amplitude modulation[25] at the focal spot in the sample, which is then detected as a delay dependent amplitude modulation of the non-collinear probe without relying on phase-matching. For instance, counter-propagating pump and probe beams, a wide-field approach, or a non-collinear probe approach, employed[27–29] in pump–probe microscopy, could, in principle, be implemented for spatially resolved MES.

As shown in Fig. 1(c), a natural extension of the partially collinear geometry is the fully collinear geometry where again the pump pulse delay induced amplitude modulation of the probe can be detected. However, in order to filter out the pump, probe, and scatter backgrounds from the signal, a combination of phase cycling, optical chopping, polarization, and spectral filtering approaches is employed. These will be further discussed in Secs. II C and II D. Assuming that the above signal filtering requirements could be met, collinear geometries naturally pave the way for MES with spatial resolution limited only by the diffraction limit of the microscope objective.

A related approach to fully collinear multidimensional spectroscopy relies on dynamic pulse-to-pulse phase cycling achieved through acousto-optic phase modulation[17,18] (AOPM) and is shown in Fig. 1(d). By uniquely tagging each optical pulse with a set radio-frequency, the specific combinations of optical pulses that lead to the nonlinear signal arise at known linear combinations of those radio frequencies, which are then filtered using phase-sensitive lock-in detection. Thus, directional filtering in a non-collinear geometry is now replaced by frequency filtering in a fully collinear geometry, as indicated in Fig. 1(d). The AOPM approach will be further discussed in Sec. II C.

Note that in all the experimental geometries considered above, interferometric phase and timing stability while scanning the time delay between the two pump pulses are necessary, especially for fast optical cycles and broadband pulses in electronic spectroscopy. Several approaches to phase-stabilized pulse-pair generation have been developed, ranging from interferometric time-delay generation with active phase stabilization,[30] passive phase stabilization through the use of a diffractive optic[31] and mechanical delay scanning in the rotating frame,[31,32] continuous stage scanning,[33] pulse shaping-based time-delay generation,[16] spatial multiplexing,[34] etc. Such approaches have been further discussed in detail in an earlier review.[13] Some of such approaches that combine the benefits of phase stability, rapid pump time-delay scanning, and facile signal filtering from the background have matured into spatially resolved techniques and will be discussed in Secs. II C and II D.

C. Pulse shaping approaches to collinear multidimensional electronic spectroscopy

The development of pulse shaping and phase-modulation approaches has been quite instrumental to the feasibility of fully collinear MES and, by extension, for advancing spatially resolved experiments. Such approaches carry a dual advantage—generation of phase-stable pulse pairs and efficient signal filtering from the collinear background. Out of these approaches, the pulse shaping approaches are discussed below. The phase-modulation approaches will be discussed in Sec. II D.

Figure 2(a) shows a typical 4*f* pulse shaper design for pulse amplitude and phase shaping in the frequency domain. The pulse shaping element typically relies on a spatial light modulator (SLM) based on either a liquid crystal array (LCA) or an acousto-optic modulator (AOM). The SLM is kept in the Fourier plane such that individual dispersed spectral components can be imparted an arbitrary spectral phase through a programmable mask. Applications of programmable pulse shaping techniques[15] to

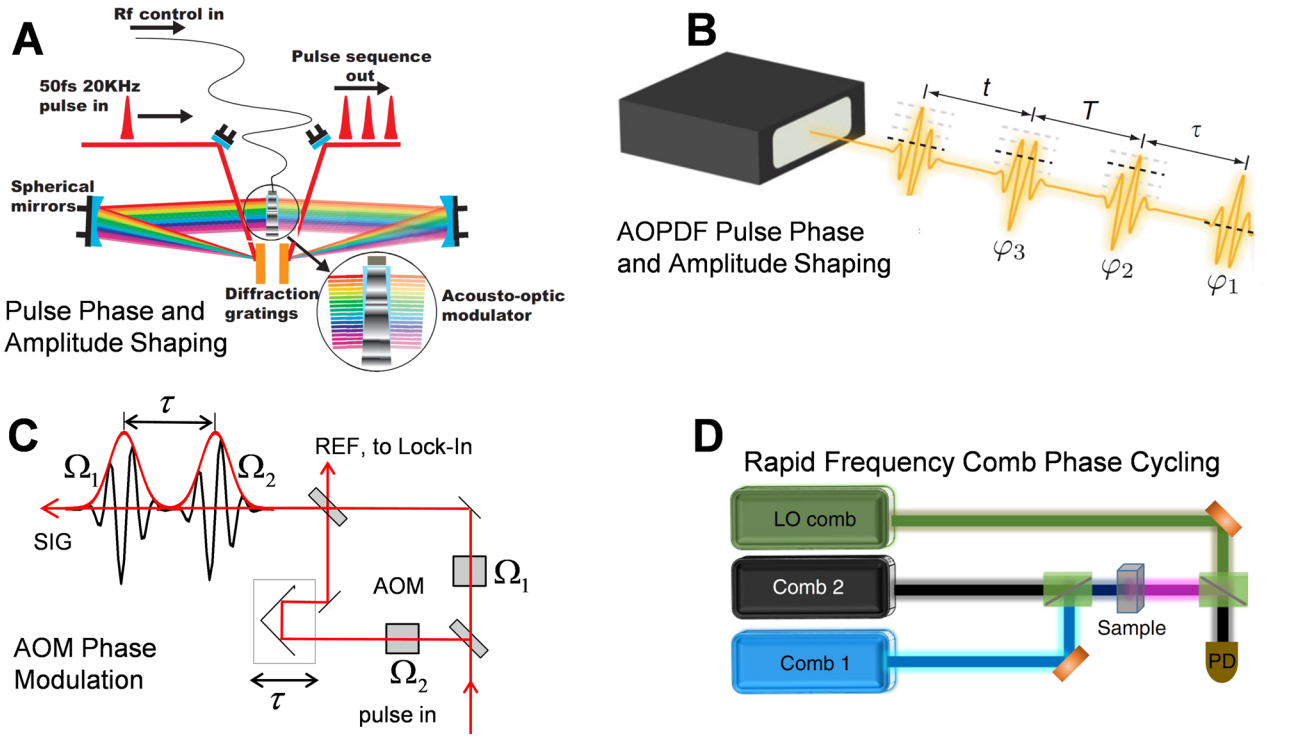

FIG. 2. Collinear multidimensional spectroscopic methods for pulse-pair phase stabilization and efficient signal filtering. (a) Acousto-optic pulse phase and amplitude shaping[16] in the frequency domain at high repetition rates[35] of up to 100 kHz. Similar implementation based on an SLM[36,37] is also possible. (b) Acousto-optic programmable dispersive filter (AOPDF)[38] based temporal phase and amplitude shaping. (c) Mach–Zehnder interferometer based pulse-pair generation. The pulse-pair is passively phase-stabilized against mechanical fluctuations using acousto-optic phase modulation (AOPM)[17] of the relative carrier–envelope phase of individual pulses in the pulse-pair. The signal (SIG) is detected relative to an optically generated reference (REF) using phase-sensitive lock-in detection, which simultaneously allows for physical undersampling of the signal. (d) Frequency combs with locked repetition rates of slightly different frequencies enable rapid time-delay scanning.[39,40] Pulse-to-pulse carrier–envelope phase cycling akin to AOPM enables frequency filtering of the heterodyne-detected signal. (a) is adapted with permission from Wagner *et al.*, Opt. Express **13**, 3697–3706 (2005). Copyright 2005 OSA. (b) is adapted with permission from Mueller *et al.*, Nat. Commun. **10**, 4735 (2019). Copyright 2019 Springer Nature. (d) is adapted with permission from B. Lomsadze, B. C. Smith, and S. T. Cundiff, Nat. Photonics **12**, 676–680 (2018). Copyright 2018 Springer Nature.

multidimensional spectroscopy have been demonstrated using both LCA- and AOM-based approaches.

Programmable pulse shaping based on LCAs and its applications in femtosecond pulse phase shaping has been pioneered by Weiner *et al.* [42] Imparting a specific computer programmable voltage mask on the LCA located at the Fourier plane of a dispersed femtosecond pulse allows for arbitrarily shaping the pulse phase with applications in coherent control[43] and femtosecond adaptive pulse compression[44] of ultra-broadband femtosecond pulses.[45] Extensions to pulse phase and amplitude shaping[46] in the Fourier domain have allowed for extensions of LCA-based femtosecond pulse shaping in MES, first demonstrated[36] by Vaughan *et al.* in a box*CARS* geometry. Using a two-dimensional LCA array, arbitrary control over individual pulse phases and relative delays was demonstrated. Feasibility of artifact suppression through cycling the relative carrier–envelope phase between individual pulses was also demonstrated. By detecting the signal in a background-free geometry, additional background suppression was not required. Later, Grumstrup *et al.* demonstrated[37] MES using LCA pulse shaping in a partially collinear pump–probe geometry. Pulse-pair phase stability comparable to that achievable through active or passive phase stabilization was measured over several hours. Note that a given pump pulse time delay is achieved by applying a sawtooth linear voltage ramp on the LCA. However, the delay scan rate is dependent on the update rate of this voltage mask, which, in turn, depends on the several milliseconds of the response time of the liquid crystals in the LCA. Thus, the experimental throughput is ultimately limited by the response time of the LCA. This can impose demanding constraints on laser and sample stability over the duration of data collection, which typically lasts several hours to complete all the phase-cycling steps for signal filtering. Further extending the LCA pulse-shaping approach to a fully collinear geometry with a 27-step phase cycling,[47] Goetz *et al.* demonstrated[48] the first spatially resolved MES experiment. These results will be discussed in Sec. III.

The AOM pulse shaping approach to multidimensional spectroscopy was pioneered[16,49] by Warren and co-workers as the true phase-cycling optical analogs of multidimensional NMR. As shown in Fig. 2(a), an AOM is placed in the Fourier plane of a 4*f* pulse shaper, and the pulse shaping is done by propagating a

programmable radio-frequency acoustic mask into the AOM crystal. The experimental throughput and bandwidth are now limited by the update rates of the acoustic mask, which, in turn, depend on the acoustic velocity of the AOM crystal. Using this approach a number of years ago, Warren and co-workers were the first to demonstrate[35,50] all-collinear collection of 2D spectra with shot-to-shot pulse shaping at repetition rates of 20 kHz only limited by the signal detection electronics. In principle, their approach is feasible for repetition rates as high as 100 kHz, where following a 16-step phase cycling[47] for signal filtering, the 2D spectrum of Rubidium (Rb) in a gas cell could be collected in as fast as 0.6 s. Their approach paved a direct path for rapid AOM pulse-shaping enabled spatially resolved multidimensional spectroscopy. Later, extending a similar AOM pulse-shaping approach to the mid-IR, Shim *et al.* demonstrated[51] phase-cycled 2D spectroscopy in the mid-IR region (2DIR) in the partially collinear geometry at 1 kHz repetition rates. Baiz *et al.* further extended[19] mid-IR AOM pulse shaping to a fully collinear geometry and demonstrated spatially resolved 2DIR. Since the probe beam was not phase-cycled, a combination of polarization filtering, pump phase cycling, probe chopping, and Fourier filtering was necessary to efficiently filter the signal from the background. Vibrational lifetime imaging was also demonstrated as a knob to enhance imaging contrast. Further extending this approach, Ostrander *et al.*[52] demonstrated a widefield 2DIR microscope implementation for spatially resolved 2DIR. Collinear pump and probe beams shaped using a dual AOM pulse shaper were used for widefield sample illumination, followed by imaging the illumination spot on a focal plane array detector. This allowed for the collection of parallel 2DIR spectra over a large sample area, significantly reducing the imaging time compared to point-scanning methods.

Recently, Luther[53] and Kearns[54] and co-workers also demonstrated multidimensional spectroscopy using 100 kHz shot-to-shot AOM pulse shaping in the mid-IR and visible regions, respectively. In the visible to NIR region spanned by white-light continuum generated pump and probe pulses, a 200-fold reduction in shot-to-shot data collection time and a reduced $1/f$ noise due to 100 kHz data collection from correlated laser shots were demonstrated. Jones *et al.* recently demonstrated[11,55] a white-light continuum 2D electronic spectrometer, which extends the 100 kHz shot-to-shot pump pulse shaping approach to spatially resolved multidimensional spectroscopy. The new science enabled by this approach will be discussed in Sec. III.

Figure 2(b) shows a related approach to shot-to-shot AOM temporal pulse shaping using an acousto-optic programmable dispersive filter[38] (AOPDF). Using the temporal pulse amplitude and phase shaping approach for the pump, Myers *et al.* demonstrated[26] two-color MES in a partially collinear pump–probe geometry and later extended[56] it to white-light continuum probing. Pump pulse phase cycling also enabled separation of different nonlinear response functions, such as rephasing and non-rephasing pathways, which are otherwise not separable in the partially collinear geometry. AOPDF-based MES with a continuum probe has also been extended to the UV region,[57] as well as employed to probe photoisomerization reaction channels.[58]

Phase-cycling theory[47] for the pump–probe geometry[59] described by Zhang *et al.* has been instrumental in the AOPDF pulse shaping approach to multidimensional spectroscopy. Some applications include fifth-order three-dimensional electronic spectroscopy[23,60] with four collinear phase-stable pump pulses generated by the AOPDF and separation of fifth-order multiple quantum[61] non-linear response pathways for observing multi-exciton correlations. Notably, Draeger *et al.* employed[62] an all-collinear *single-beam* 1 kHz shot-to-shot AOPDF pulse shaping to demonstrate multi-quantum multidimensional action spectroscopies. Overall, the development of AOM $4f$ pulse shaping and AOPDF approaches has enabled rapid time-delay scanning with phase-stable pulses and efficient signal filtering from the background. Together, these features have spurred the development of all-collinear higher-order and action-based multidimensional spectroscopies (Sec. II E). The high-throughput and sensitivity of 100 kHz shot-to-shot AOM pulse shaping[54] have also been quite instrumental in the development of spatially resolved MES. These techniques, and the new science enabled by it, will be discussed in Secs. II E and III.

D. Phase modulation approaches to collinear multidimensional electronic spectroscopy

The pulse shaping based all-collinear approaches discussed in Sec. II C rely on both amplitude shaping to scan the time delays between phase-stable pulses and cycling the relative carrier–envelope phase of individual pulses from 0 to 2π in order to filter the signal against the background. In contrast, generating phase-locked collinear pulses using traditional interferometric techniques requires active phase stabilization[24,63] using phase-locked loops. As a result, time-delay scanning becomes much slower and therefore susceptible to long-term laser noise. Furthermore, reliably filtering the signal against the background also becomes challenging. Thus, rapid shot-to-shot pulse shaping techniques, even though ultimately limited by the update rate of the AOM acoustic mask, are highly desirable over traditional interferometric generation of phase-locked pulse pairs for collinear MES. Rapid shot-to-shot phase cycling is especially desirable for spatially resolved measurements where sample photostability constraints are demanding.

To this end, an effective substitute to pulse shaping techniques is the phase-modulation approaches to multidimensional spectroscopy. Here, the relative carrier–envelope phase is dynamically cycled either using AOM-based radio-frequency phase modulation[17,18] [AOPM approach in Fig. 2(c)] or through the use of carrier–envelope phase-stabilized frequency combs[39,40,64] [Fig. 2(d)]. These techniques are therefore not limited by the update rates of the AOM pulse shaping mask and at the same time capable of rapid time-delay scanning[65] of phase-stabilized pulse pairs.

1. AOPM based

Tekavec and co-workers pioneered[17,18] the AOM phase-modulation (AOPM) approach to multidimensional spectroscopy. Below, we discuss that the AOPM approach offers several unique advantages over both traditional interferometric techniques and pulse-shaping approaches discussed in Sec. II C.

As shown in Fig. 2(c), the time-delay generation in the AOPM approach is based on Mach–Zehnder (MZ) interferometers with no active phase stabilization. However, each arm of the MZ interferometer is tagged with a slightly different AOM radio-frequency. The

relative carrier–envelope phase in each arm of the interferometer is then phase-modulated at the respective AOM radio-frequency. Because of the relative difference in the phase modulation in each arm, the output pulse-pair is amplitude modulated at the difference of the radio-frequencies of each arm. This amplitude modulation is ultimately carried over to the signal detection, which can be either heterodyned[65,66] or action-based.[18] The differences in signal detection will be discussed in Sec. II E. Crucially, the second MZ port or an additional reference laser traveling through the same optical path is used to generate an optical reference, and the signal is then detected with respect to this optically generated reference frequency using phase-sensitive lock-in detection. As shown in Fig. 1(d), the specific directionally filtered four-wave mixing signals in the non-collinear approach are now replaced by four-wave mixing signals modulating at specific linear combinations of the unique AOM radio-frequencies, which are then filtered using phase-sensitive lock-in detection.

Overall, a combination of phase modulation, signal detection relative to an optical reference frequency, and phase-sensitive lock-in detection provides the following advantages: (1) Physical undersampling of the signal made possible by signal detection in the rotating frame of the reference frequency. This is similar to rotating frame phase cycling,[47] which allows for undersampling of the optical frequency and therefore faster data collection. (2) Rotating frame detection also leads to passive phase stabilization because mechanical fluctuations in delay lines now result in significantly smaller phase fluctuations. Additionally, the optical reference tracks the relative phase fluctuations in the signal due to mechanical jitter and phase-sensitive lock-in detection relative to the reference cancels such fluctuations in the signal. Thus, the radio-frequency imparted carrier–envelope phase on each pulse is effectively decoupled from mechanical fluctuations in the unstabilized interferometer. (3) Dynamic phase-cycling and lock-in frequency filtering do not depend on acoustic velocity dependent mask update rates.

Tekavec *et al.* first demonstrated the feasibility of the above AOPM approach for quantum wavepacket reconstruction[17] and multidimensional spectroscopy.[18] Lavoie *et al.* recently applied the AOPM approach in the context of entangled two-photon interference.[67] In addition to the above described advantages of this approach, Autry *et al.* recently demonstrated[65] a rapid time-delay scanning AOPM approach, making it comparable to AOM pulse-shaping approaches in terms of experimental data collection time. The AOPM approach to collinear MES thus carries unique advantages in terms of experimental throughput, acoustic mask update rate independent dynamic phase cycling, and phase-sensitive lock-in detection, making it an attractive route toward srMES. The new science enabled by the AOPM approach will be discussed in Secs. II E and III.

2. Optical frequency comb-based

Recent application[39,40,64] of carrier–envelope phase-stabilized frequency combs[68] to multidimensional spectroscopy has been a promising development. Using two frequency combs with locked repetition rates of slightly different frequencies, Lomsadze[39,40] and Kim[64] and co-workers demonstrated that locking the slightly different repetition rates of two frequency combs can serve as a way for rapid time-delay scanning between the two combs, where the time-delay scan rate is proportional to the frequency difference between the combs. Because the carrier–envelope phase is incrementally swept between successive comb lines, this technique is, in principle, similar to the AOPM approach, allowing for repetition rate independent pulse-to-pulse phase cycling.

Since the delay scan only depends on the repetition rate difference between the combs, no mechanically moving parts are necessary to scan the delay. As shown in Fig. 2(d), Lomsadze *et al.* demonstrated[40] ultra-high resolution frequency comb multidimensional spectroscopy with no mechanically moving parts in an all-collinear geometry. The time delays between the first two pulses and the signal and the local oscillator could be scanned for as long as nanoseconds. The scan range is essentially set by the repetition rate of the frequency comb, and the scan rate is set by the slight difference in repetition rates. With no mechanically moving components, each 2D spectrum could be obtained in as short as ~0.3 s. The background filtering of the signal can be done in the frequency domain because the signal appears at specific linear combinations of the three input comb lines and the local oscillator comb line. The new science enabled by these measurements will be discussed in Sec. II E.

E. Action-based multidimensional electronic spectroscopy

Warren and Zewail first demonstrated[69] the feasibility of manipulating the phase of optical pulses through the use of easily controllable radio-frequency phases, similar to what is known in NMR. Using this technique, the phase of the last pulse in a photon-echo experiment could be manipulated to convert a third-order oscillating nonlinear polarization into an incoherent "action" [70] signal, which is proportional to the excited state population and carries the time-delay dependent amplitude and phase information of the third-order polarization. Tian *et al.* demonstrated[50] fluorescence-detected MES using AOM phase cycling discussed in Sec. II C. The AOM phase-cycling technique was later demonstrated[35] by Wagner *et al.* to be feasible for simultaneously collecting both coherent and action-based 2D signals from the Rb gas cell, with shot-to-shot phase cycling at repetition rates as high as 100 kHz.

As discussed in Sec. II D, Marcus and co-workers demonstrated an alternate approach to fully collinear MES based on AOPM. Using the AOPM approach, Tekavec *et al.* demonstrated[17] quantum electronic wavepacket reconstruction on Rb, where complex susceptibility can be easily recovered compared to earlier wavepacket interferometry experiments[71] using actively phase-locked pulse pairs. The same approach was further extended[18] to fluorescence-detected MES of Rb vapor.

From these initial demonstrations, the action-based MES (aMES) approach has enabled several new insights. As shown in Fig. 3(a), Lott *et al.* determined[72] the average ground state conformation of porphyrin dimers self-assembled in a membrane environment. Constrained fitting of the linear absorption spectrum and the 2D spectrum could determine the separation and angles between transition dipoles. Through simulations of four-wave mixing pathways, they also showed that aMES shows qualitatively different signatures compared to heterodyne-detected MES (hMES) due to additional excited state absorption (ESA) pathways in aMES, which can destructively interfere to result in only the ground state bleach (GSB)

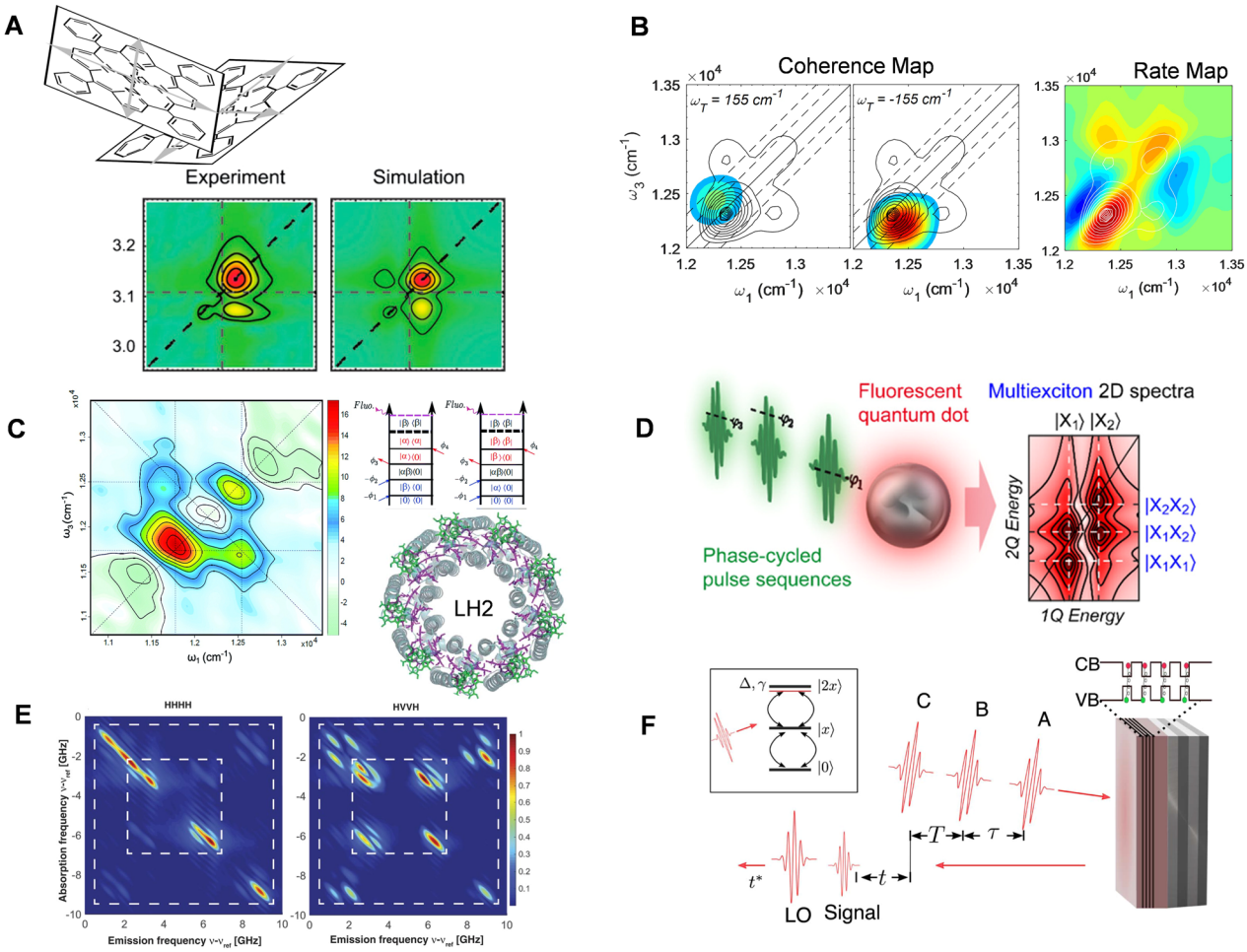

FIG. 3. Some examples of all-collinear heterodye-detected (hMES) and action-based (aMES) variants of multidimensional electronic spectroscopy (MES). (a) Determination of ground state conformation of porphyrin dimers self-assembled in a phospholipid bilayer membrane using fluorescence-detected aMES. Adapted with permission from Lott *et al.*, Proc. Natl. Acad. Sci. U. S. A. **108**, 16521–16526 (2011). Copyright 2011 National Academy of Sciences. (b) Determination of the ultrafast rate and coherence maps in a strongly coupled bacteriochlorin dyad at room temperature using fluorescence-detected aMES. Adapted with permission from Tiwari *et al.*, Opt. Express **26**, 22327–22341 (2018). Copyright 2018 OSA. (c) Determination of exciton correlations between the B800 and B850 bands of the LH2 antenna complex using fluorescence-detected double-quantum coherence aMES. Adapted with permission from Karki *et al.*, Chem. Sci. **10**, 7923–7928 (2019). Copyright 2019 the Royal Society of Chemistry. (a)–(c) employ the AOPM approach to collinear MES and rely on incoherent or action-based detection. (d) Multiexciton correlations, binding energies, and transition moments in colloidal core–shell quantum dots were measured using multiple quantum aMES. The approach employs AOPDF-based shot-to-shot phase cycling at 1 kHz. Adapted with permission from Mueller *et al.*, ACS Nano **15**, 4647 (2021). Copyright 2021 American Chemical Society.[77] (e) Frequency comb-based hMES 2D spectra of Rb vapor. The high frequency resolution provided by frequency combs resolves Rb^{85} and Rb^{87} isotopes, as well as inter-atom interactions between the same isotopes in the presence of high-temperature Doppler broadening. Adapted with permission from B. Lomsadze and S. T. Cundiff, Science **357**, 1389–1391 (2017). Copyright 2017 AAAS. (f) Rapid-scan hMES variant of the AOPM approach characterizes all the multiple quantum four-wave mixing pathways in GaAs/AlGaAs quantum wells in a single scan. Adapted with permission from Autry *et al.*, Optica **6**, 735–744 (2019). Copyright 2019 OSA.

and excited state emission (ESE) pathways. Ultrafast electronic population transfer[73] and the interplay[74] of energetically vs thermodynamically favored conformations in self-assembled dimers were also studied in later experiments. The capability of the fluorescence-detected AOPM approach to determine dimer conformations has also been extended[75] in the UV region to study the conformations of dinucleotide dimer models.

Nardin *et al.* extended the AOPM aMES approach to coherent nonlinear photocurrent measurements[78] on epitaxially grown coupled quantum well systems. Karki *et al.* also applied[79] the AOPM approach to aMES on a semiconductor quantum dot based photocell to probe sub-picosecond multiple exciton generation.[80] This experiment exploits the two unique features of aMES as applicable to multiple exciton generation—the cancellation between extra ESA pathways in aMES is sensitive to the Auger recombination between multiple electron–hole pairs, which can be altered in a photocell, and both nonlinear fluorescence and photocurrent measurements can be measured in action-based measurements. Yang *et al.* used the

AOPM approach to compare linear photocurrent and two-photon photoluminescence maps from thin-film perovskites to map trap-state distributions.[81] Using the AOPM approach, Vella *et al.* also performed[82] photocurrent aMES on organic photovoltaic systems. Crucially, they highlighted[83] an inherent complexity associated with incoherent action-based detection in MES, which is that the non-geminate recombination between excitons in uncoupled systems can also lead to cross-peaks in the aMES 2D spectra. Similar and additional effects such as detector saturation have also been proposed[84] to contribute at the desired signal frequency in an action-detected four-wave mixing signal. This will be further showed in Fig. 4, which highlights the fundamental differences between 2D spectra expected from hMES vs aMES approaches. Further extending the AOPM approach to aMES, Tiwari *et al.* measured[76] long-lived room temperature vibrational wavepackets in a strongly coupled bacteriochlorin dyad in the form of 2D maps of coherent waiting time dynamics [Fig. 3(c)]. These wavepackets survive the sub-picosecond electronic relaxation in the dyad. Analysis of 2D maps reveals that the vibrational wavepackets most likely arise from multiple vibrational levels on the ground electronic state.

Recently, as shown in Fig. 3(c), Karki *et al.* reported 2D cross-peaks in a double-quantum aMES experiment on the multichromophoric purple bacterial light-harvesting complex (LH2). The double-quantum 2D spectrum can reveal[85] exciton–exciton correlations, for example, between the two bacteriochlorophyll rings found in the LH2 complex. Given the complexity[86] of additional pathways contributing at the same signal frequency as the desired four-wave mixing pathways, 2D cross-peaks in aMES are actively investigated.[86–88] It becomes crucial to understand how exciton–exciton interactions influence the four-wave mixing pathways contributing to aMES.

Introducing multiple spectral dimensions through higher-order light–matter interactions and investigating higher than one-quantum coherences, similar to double-quantum coherence experiments,[20] are two possible approaches to disentangle exciton–exciton interactions influencing action-detected 2D signals. In this context, the AOPDF-based 1 kHz shot-to-shot pulse-shaping approach to aMES, developed[62] by Draeger *et al.*, has been quite instrumental. The flexibility of the single-beam AOPDF experiment to produce programmable multiple pulse orderings and phase cycles on a 1 kHz shot-to-shot basis has been exploited by Mueller *et al.*[89] to perform multiple quantum aMES, which can reveal[85] exciton–exciton correlations. A 16-step phase cycling separates the non-linear response pathway, exclusive to aMES,[47] to reveal the energy shifts between a two-quantum excitation vs two one-quantum excitations. As shown in Fig. 3(d), Mueller *et al.* recently applied a 36-step phase-cycling technique to measure bi-exciton binding energies in alloyed semiconductor core–shell quantum dots. Comparisons with response function simulations also determined relative transition dipole strengths of excitons and bi-excitons, as well as anti-correlated transition energy fluctuations between ground and single-exciton states compared to transitions from single-exciton to multi-exciton states.

Fifth-order hMES techniques that utilize AOPDF pulse shaping in a partially collinear geometry to reveal exciton–exciton many-body correlations were demonstrated[90] by Dostál *et al.* Extending aMES from fourth-order to a sixth-order technique, Brixner and co-workers recently applied a 125-fold phase-cycling variant of the above approach, which can filter the sixth-order non-linear response pathways. These pathways arise from two simultaneous interactions from each of the two pump pulses such that the resulting signals may reflect many-body interactions between two populations in coupled multichromophoric systems. Further details of the AOPDF approach to aMES can be found in another review.[91]

In parallel to the developments in AOPDF pulse shaping approaches toward all-collinear aMES, promising advancements in the phase-modulation approaches to MES (Sec. II D) have also been made. As discussed in Sec. II D, the development of frequency comb-based all-collinear MES with a 2D data collection time of as short as 0.3 s is a promising development that may also advance into spatially resolved MES (Sec. III). However, the applicability of comb-based spatially resolved measurements on condensed phase systems using broadband few-cycle pulses typical in other 2DES experiments presents its own set of challenges, which are discussed briefly in Sec. IV. Figure 3(e) exemplifies the unprecedented frequency resolution and high experimental throughput available in comb-based MES. The frequency resolution was sufficient to distinguish two Rb isotopes, as well as reveal cross-peaks, indicating many-body intra-isotope interactions in the presence of Doppler broadening. With regard to the AOPM approach, recently demonstrations of hMES variants[66] of original action-based AOPM experiments, as well as rapid-scan hMES variants[65] [Fig. 3(f)], which can collect all four-wave mixing pathways in a single scan, are promising developments in the context of srMES discussed in Sec. III. Note that apart from the above approaches, a non-collinear LCA phase-cycling approach toward fluorescence-detected MES, relying on imaging a dynamic grating, has also been demonstrated[92] on a laser dye.

Action-based MES in the gas phase has been exemplary with regard to demonstrations of greater signal sensitivity achievable through incoherent population detection. Recently, Roeding and Brixner coupled[93] a mass spectrometer to detect the photoionized population generated from a NO_2 molecular beam excited with four collinear pulses shaped by using an AOPDF. The resulting photoionized population is recorded as a function of inter-pulse time delays to yield the aMES spectra of gas phase samples. This has not been achievable through conventional hMES methods due to insufficient detection sensitivity of the radiated electric field. Bruder *et al.* integrated[94] the AOPM approach to aMES to study weak interactions between Rb atoms doped in a Helium (He) nanodroplet. The signal sensitivity was sufficient to measure weak interactions in Rb_2 and Rb_3 "molecules" within the He matrix, dynamic Stokes' shift induced by the He bath, and ultrafast population transfer and associated coherent wavepackets within the Rb "molecules." Recently, fluorescence-encoded infrared (FEIR) measurements[95] from the work of Whaley-Mayda *et al.* have also suggested enhanced sensitivity of action-based signal detection down to 1 nM concentrations. In the context of enhanced sensitivity of action-based signals, it would be interesting to compare aMES sensitivity to comb-based MES,[40] where a coherently detected signal can still be well resolved on account of noise reduction and signal averaging provided by ultra-rapid data collection. In the same context, it is worth noting that hMES extensions[65,66] of the AOPM approach rely on optical amplification of the weak signal field through the use of an intense LO, which does not pass through the sample. Since the resulting

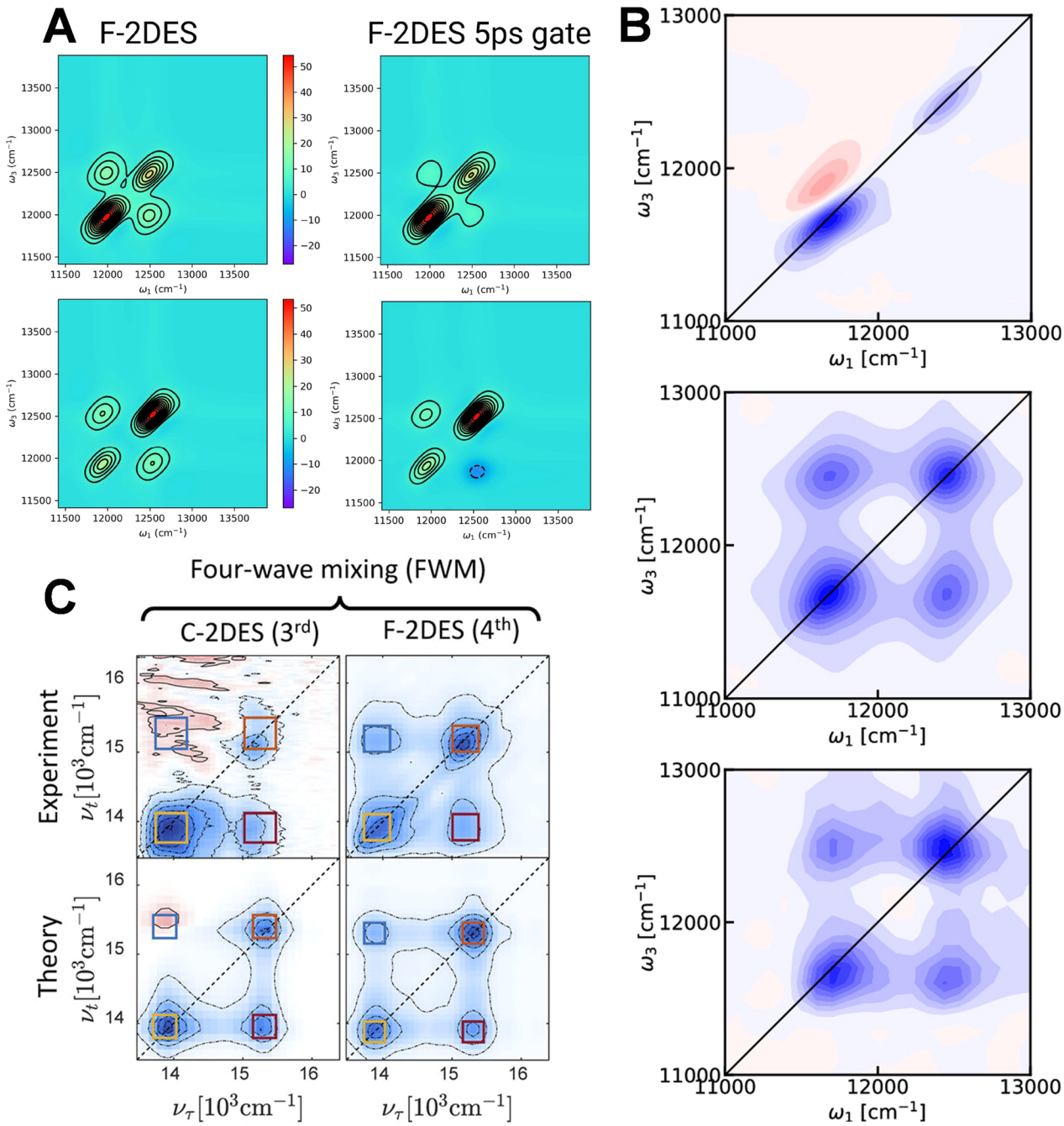

FIG. 4. New theoretical insights into aMES. (a) Exact cancellation between excited state absorption (ESA) pathways in aMES experiments is possible through exciton–exciton annihilation (EEA), revealing a clean ESA-free 2D spectrum.[72] For a dimer system, it is shown[96] that gated fluorescence detection before EEA can reveal the ESA cross-peaks canceled out in time-integrated fluorescence detection. Adapted with permission from P. Malý and T. Mančal, J. Phys. Chem. Lett. **9**, 5654–5659 (2018). Copyright 2018 American Chemical Society. (b) Theoretical simulations of action-2D spectra resulting from EEA in larger aggregates, such as the LH2 photosynthetic antenna complex, also explain the experimentally observed apparently "homogeneous" line shapes. The experimental 2D spectrum is shown in the lower panel, the fluorescence-detected spectrum is shown in the middle panel, and the heterodyne-detected 2D spectrum is shown in the upper panel. Adapted with permission from Kunsel *et al.*, J. Phys. Chem. B **123**, 394–406 (2019). Copyright 2019 American Chemical Society.[97] (c) Direct experimental comparisons[86] of heterodyne 2D and action-2D spectra of squaraine heterodimers enabled by the AOPDF-based temporal phase and amplitude shaping approach. Adapted from Malý *et al.*, J. Chem. Phys. **153**, 144204 (2020) with the permission of AIP Publishing.

detection is lock-in-based, fringe contrast between the LO and the signal field interference is not a constraint, assuming that the photodetector has a sufficient dynamic range. Optical amplification of a weak signal field may thus potentially enhance the sensitivity of heterodyne detection.

Owing to enhanced signal sensitivity, some of the above approaches to fully collinear MES have enabled the development of srMES, which will be discussed in Sec. III. However, before a discussion of spatially resolved experiments, a brief highlight on the recent understanding of the differences between hMES and aMES 2D spectra is warranted. This has been enabled through a close synergy between both, theoretical simulations of the nonlinear response functions contributing to MES and direct experimental comparisons between the two approaches. As shown in Fig. 3(a), Lott *et al.* pointed[72] out the extra ESA wave mixing (ESA II) pathways involving multi-exciton states, which are available in aMES. The additional ESA pathways are oppositely signed compared to hMES-type ESA (ESA I) pathways such that exciton–exciton annihilation may lead to an exact cancellation of ESA pathways in aMES experiments. Note that an exact cancellation of ESA pathways relies on perfect efficiency of exciton–exciton annihilation[98] such that multi-exciton states have the same fluorescence quantum yield as the lowest exciton state. Such an assumption may not hold true for dyads[76,99] where, unlike a purely excitonic dimer, singly excited electronic states can have different symmetries.

Simulating a purely excitonic dimer, Mancal and co-workers suggested an interesting possibility of time-resolving the interpulse delay dependent incoherent fluorescence signal, for instance, through a time-gated fluorescence detection. As shown in Fig. 4(a), when the fluorescence is gated at half the timescale of exciton–exciton annihilation, then 2D cross-peaks in the weakly coupled case (top row) are reduced compared to when the fluorescence is time-integrated by using the detector. This suggests that 2D cross-peaks in the time-integrated case reveal a clean GSB+ESE signal[100] because perfect annihilation allows for exact cancellation between ESA I and ESA II signals. The same qualitative trend holds for the strong electronic coupling case as well. Jansen and co-workers simulated the 2D spectrum of the multichromophoric LH2 protein complex. As shown in Fig. 4(b), a good agreement between the "homogeneous" line shapes obtained in the fluorescence-detected experiments (bottom row) and the simulated spectrum (middle row) is obtained. Their findings suggest that, in the case of perfect exciton–exciton annihilation, aMES spectra do not reveal frequency–frequency correlations between the excitation and detection frequencies. The hMES spectrum (top row) shows quantitatively different features for the same reasons as those suggested by others.[70,72,96,100] Recently, Kalaee *et al.* suggested[87] that exciton–exciton annihilation pathways, such as ESA II, can be distinguished based on their opposite sign, which can be experimentally reconstructed from linear fluorescence signals. Malý *et al.* directly compared[86,88] the aMES and hMES spectra of squaraine heterodimers shown in Fig. 4(c), revealing good agreement of experiments with purely excitonic dimer models with perfect exciton–exciton annihilation for the case of squaraine heterodimers. They also reported[88] sixth-order aMES[41] on these dimer systems to extract the response function pathways specific to bi-exciton annihilation.

Overall, a combination of the above theoretical and experimental findings has enriched the understanding of action-detected 2D signals, as well as spurred the development of new MES approaches in order to understand the exciton annihilation pathways contributing to aMES.

III. SPATIALLY RESOLVED MULTIDIMENSIONAL ELECTRONIC SPECTROSCOPY

The technological progress that has enabled new methodologies for all-collinear MES has naturally paved the way for introducing spatial resolution in multidimensional spectroscopy. Below, we discuss some of the recent applications of srMES based on the approaches discussed in Sec. II. We also highlight the new science that has already been enabled through the introduction of spatial resolution in an already powerful spectroscopic tool.

Figure 5(a) shows an earlier action-detected approach[101] to srMES where the enhancement of spatial resolution is not determined by the laser illumination spot, but rather by high spatial resolution imaging of photoelectron emission. A collinear pulse train of 4 fs pulses is generated through LCA pulse shaping. The spatial origin of photoelectron yield after sample illumination is mapped with ~50 nm resolution as a function of inter-pulse time delays to obtain the Fourier transform 2D spectrum. The spatial resolution and sensitivity were sufficient to correlate sub-diffraction limit variations on an Ag surface to differences in the corresponding 2D line shapes. Spatial differences in coherences along the waiting time T were reported to arise from different hotspots and attributed to coupling between local surface plasmon modes. Recently, the above approach has been integrated[102] into a multifunctional photoelectron microscope-based spectrometer.

Recently, Goetz *et al.* extended[48] the above LCA pulse shaping approach to integrate it with a confocal microscope, which combines aMES with 12 fs time resolution and ~260 nm diffraction-limited spatial resolution. The LCA phase-cycling approach demonstrated robust phase stability over several hours required to complete the 27 phase cycles to collect a 2D spectrum of individual aggregated structure in an organic thin film. As shown in Fig. 5(b), Li *et al.* reported[103] variations in nanoscale coherence length and correlated it with the topology within these individual structures or "molecular islands," offering an interesting perspective on engineering local topology to achieve enhanced coherence lengths. Their approach relies on the simultaneous measurement of the linear fluorescence excitation spectrum map of these structures along with the 2D spectra. Very recently, Li *et al.* also reported[106] coherent phonons with waiting time measurements on single-layer MoS_2. Simulating these observations allows for the estimation of the room temperature exciton–phonon coupling strengths.

As shown in Fig. 3(c), Ogilvie and co-workers extended the AOPM dynamic phase-cycling approach to aMES by combining it with a point-scanning confocal microscope. The 2D spectrum at specific points of this confocal map can be collected within a few seconds. Purple bacterial cells grown under high and low-light conditions show[107] subtle variations in their linear absorption spectrum, which reflect perturbations to the excitonic structure caused by low-light growth. The sensitivity of non-linear fluorescence-detected signals was sufficient to distinguish these changes across different

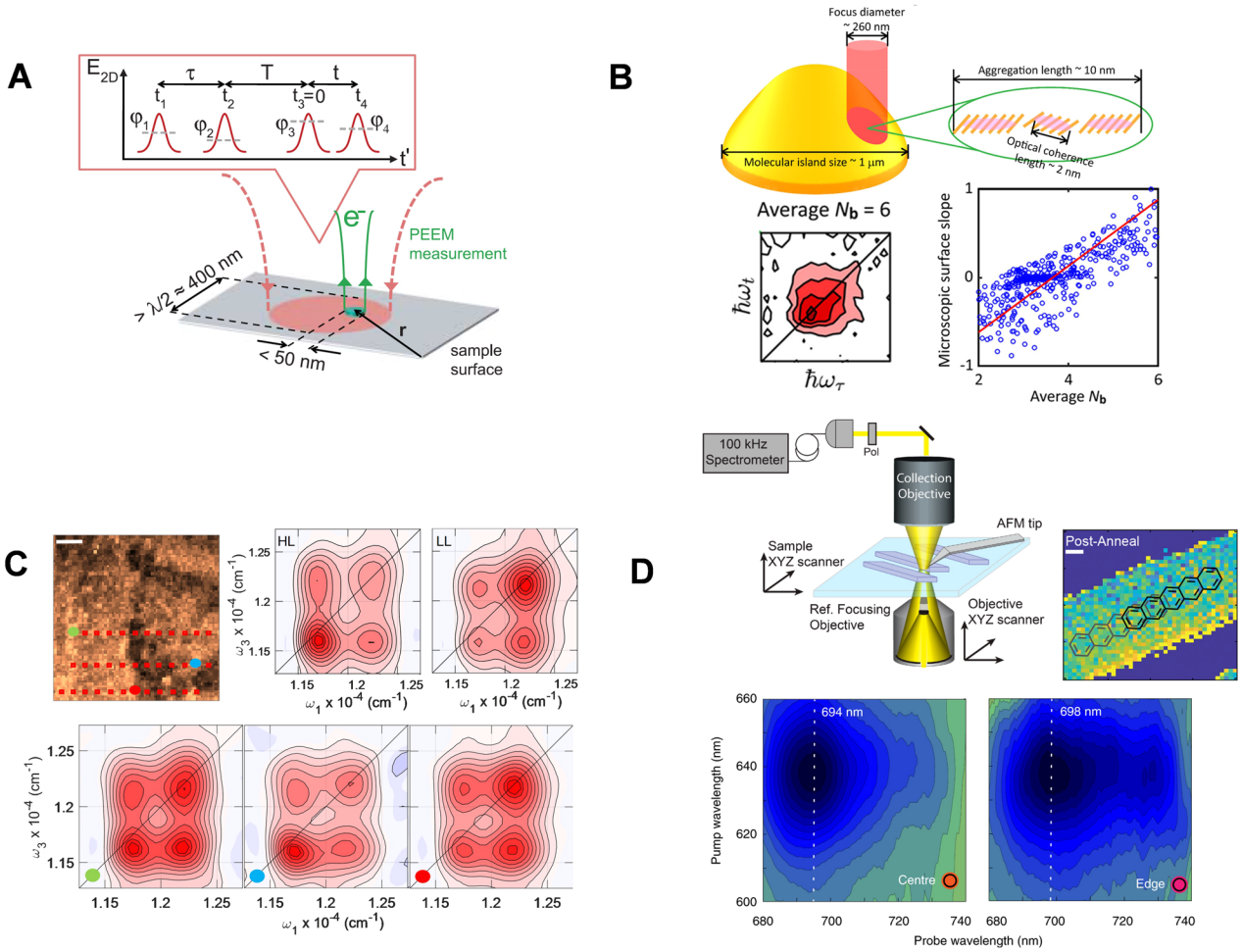

FIG. 5. New directions enabled by srMES. (a) Coherent 2D nanoscopy.[101,102] Combining photoelectron emission microscopic (PEEM) imaging with LCA pulse shaping based aMES enables sub-diffraction limit imaging of nanostructures. Adapted with permission from Aeschlimann *et al.*, Science **333**, 1723–1726 (2011). Copyright 2011 AAAS. (b) LCA pulse shaping based aMES and fluorescence excitation spectrum measurements resolve spatially varying coherence length inside molecular aggregates in an organic thin film. Adapted with permission from Li *et al.*, Nano Lett. **20**, 6452–6458 (2020). Copyright 2020 American Chemical Society. (C) AOPM-based srMES approach demonstrated that differences in the excitonic structure of spatially heterogeneous samples, such as a mixture of high vs low-light grown purple photosynthetic bacteria, can be spatially resolved on a 2D map with high sensitivity of fluorescence detection. Adapted with permission from Tiwari *et al.*, Nat. Commun. **9**, 4219 (2018). Copyright 2018 Springer Nature. (d) 100 kHz shot-to-shot pulse shaping enabled srMES correlated with AFM topographic imaging of sample morphology identifies non-equilibrium molecular packings, which favor singlet exciton fission through increased charge-transfer couplings. Adapted with permission from Jones *et al.*, Nat. Chem. **12**, 40–47 (2020). Copyright 2020 Springer Nature; Jones *et al.*, J. Phys. Chem. A **123**, 10824–10836 (2019). Copyright 2019 American Chemical Society; and Armstrong *et al.*, J. Phys. Chem. C **124**, 15123–15131 (2020). Copyright 2020 American Chemical Society 2020.

points of a sample of mixed low-light and high-light grown purple bacteria.

Following the frequency-domain AOM pulse shaping approach [Fig. 1(a)], Jones *et al.* demonstrated[55] a fully collinear pump–probe approach to hMES with 100 kHz shot-to-shot pulse shaping.[54] As shown in Fig. 5(d), a retractable AFM tip correlates the srMES measurements with the corresponding nanomorphology. Jones *et al.* recently applied[11] their approach to demonstrate that edges of pentacene microcrystals exhibit linear and 2D spectra consistent with a red-shifted singlet state. Spectral modeling reveals that this is consistent with non-equilibrium slip-stacked packing at the edges, which is controllable through thermal annealing,[105] and promotes mixing of singlet-states with charge-transfer states, leading to the observed red-shifted shoulder. They reported enhanced singlet exciton fission rates resulting from these mixed states at the microcrystal edges, offering a direct connection between morphology and favorable energetics.

IV. FUTURE PROSPECTS

Although the demonstrations of srMES using a diffraction-limited laser spot have recently been fair, the promise of this

approach is evident from the exciting scientific possibilities already demonstrated by combining spectral, temporal, and spatial resolutions. The invention of Fourier transform MES[108] and its subsequent developments[13] have almost paralleled the developments of super-resolution microscopy techniques[109] although in very different contexts. Significant advancements have also been made in the fields of plasmon-enhanced Raman spectroscopies.[110] From the above discussion, it is clear that the path forward for srMES hinges not on one key development or a particular approach, but rather on continued developments in experimental throughput, signal detection sensitivity, and spatial resolution. In the context of current challenges, below, we discuss some of the prospective approaches motivated from the parallel developments in other spectroscopies, along with certain outstanding scientific questions, which ultimately propel further improvements in srMES.

A. Toward higher signal sensitivity

Continued developments in surface-enhanced Raman scattering experiments have shown several orders of magnitude Raman scattering enhancement from metallic substrates.[110] Substrates have ranged from roughened silver or gold surfaces to nanoparticles and metallic tips. Detection sensitivities at the level of single-molecule detection[111] are comparable to single-molecule fluorescence detection. Furthermore, measurements[112] of Raman vibrational wavepackets from a single-molecule placed near a gold nanodumbell demonstrate sensitivities ranging beyond typical single-molecule fluorescence detection.

The idea of using a metallic nanoparticle substrate to achieve the near-field enhancement of incident electric fields and the enhancement of far-field scattered radiation has already been carried over in the 2DIR community with exciting recent developments. These include the 3–4 orders of magnitude signal enhancements from few nanometer thick organic monolayers on continuous[113,114] and gold nanoantenna patterned substrates.[115] In the mid-IR, a reduced near-field enhancement[115,116] is expected at plasmon resonance. In contrast, implementing such schemes in hMES, in the visible electromagnetic region, lends promise in terms of significantly higher near-field signal enhancements comparable to those observed in surface-enhanced coherent anti-Stokes Raman scattering,[110] scaling with fourth power of the near-field enhancement $|E|^4$. Furthermore, the issue of narrowband mid-IR plasmon resonances leading to distorted Fano line shapes,[115,116] which also depend sensitively on the spectral position relative to the plasmon resonance, may be reduced for broadband plasmon resonances in the visible frequency region.

The near-field enhancement caused by surface plasmon resonances can be especially relevant for aMES-based approaches. As opposed to metal-induced fluorescence quenching at very short distances, by tuning metal–fluorophore distance through the use of dielectric spacers,[117,118] up to two orders of magnitude average enhancement of fluorescence quantum yields from organic monolayers have been demonstrated. Such an approach when integrated with aMES promises a key additional benefit of significant enhancements of fluorescence quantum yields of non-fluorescent monolayers, which proportionally scale the overall signal in addition[117] to the $|E|^4$ average near-field enhancement. It is also known that plasmonic fluorescence enhancement occurs through faster radiative decay rates, outcompeting non-radiative decay channels. For example, 5.5× higher fluorescence quantum yield correlated with an ~50 times faster radiative decay rate[119] for an isolated photosynthetic protein close to a nanoantenna. In addition to the signal enhancement, the altered excited state dynamics[120] caused by surface plasmon resonances could also be leveraged to possibly prevent aMES signal cancellations caused by exciton–exciton annihilation in multichromophoric systems (Sec. II E), effectively similar to theoretically proposed gated fluorescence detection (Fig. 4). Thus, while plasmonic signal enhancement offers promising benefits for hMES, it offers additional unexplored avenues for pushing the detection sensitivity of fluorescence-based aMES approaches beyond the current state of the art.

B. Beyond diffraction-limited spatial resolution

In this context, a plethora of tools from super-resolution microscopy are available to ultrafast spectroscopists, such as shaped beams[121] as in stimulated-emission depletion microscopy (STED) or apertured fiber based probes in near-field optical microscopy[122] (NOM), with an available spatial resolution down to ~100 nm. However, issues related to photobleaching in STED and poor coupling efficiencies (>0.01%) in fiber apertured probes do not offer a straightforward implementation for broadband femtosecond pulses with low pulse energies available in the 0.1–1 MHz range. Moreover, the four-wave mixing point spread function in srMES is already more confined[104] than a typical point spread function of ~200 nm in linear confocal imaging, implying that approaches with spatial resolution down to a few tens of nanometers may be more relevant.

In this context, near-field enhancements near plasmonic hotspots such as the nanoantenna tips[110] carry a dual advantage. Hotspot associated near-field enhancements are reported to be larger compared to the average near-field enhancement near a metallic surface. For example, organic molecules embedded in a dielectric polymer layer coated on a lithographically fabricated bowtie nanoantenna substrate have reported[123] ~1340 times enhancement of fluorescence on account of larger absorption rates and faster radiative lifetimes. The additional advantage of nanoantenna hotspots is the highly confined electric fields in the nanoantenna tip–sample junction upon illumination of the junction by far-field light. However, despite desirable spatial resolution down to a few tens of nanometers, signal separation from large far-field background often requires a combination of interferometric and lock-in detection as in pump–probe NOM[124] and may not be amenable to integration with typical srMES experiments.

Taking this concept of nanoantenna a step further, tapered metallic tips have been demonstrated as mode-matching waveguides for far-field/near-field coupling through the use of a grating[125] or slit[126,127] structure on the tapered metallic tip, with theoretical coupling efficiencies[128] of ~50%. Demonstrations of plasmonic nanofocusing of femtosecond pulses and octave spanning white light[126,127] down to ~10 nm have been extremely promising because of the possibility of near-field signal enhancements without any far-field illumination background. In particular, nanofocusing femtosecond pulses with coupling efficiency high enough to generate second-harmonic[129] or four-wave mixing[130] non-linear signals from the nanoantenna tip, along with phase and amplitude control[129] over

the resulting waveforms, underscore the impending applicability of these approaches to srMES. Although current surface plasmon polariton (SPP) based nanofocusing approaches have demonstrated coupling efficiencies of only >10%, these efficiencies are already significantly higher than fiber aperture based NOM. It is noteworthy that recently,[131] a combination of metallic nanowire and optical fiber based nanofocusing has demonstrated the total excitation and collection efficiency of ~50%, measured for narrowband continuous wave light sources in the visible region and substantially higher than typical fiber aperture based or SPP based NOMs discussed above.

C. Faster throughput

From the various approaches discussed in Sec. II, it is evident that all-collinear frequency comb-based techniques, which may be relevant for srMES, do not rely on any mechanically moving parts to offer the highest throughout in terms of rapid delay scanning. However, in typical condensed phase systems, frequency resolution is system limited and not the primary requirement. Reduced repetition rates in order to minimize sample photodegradation, signals from unrelaxed electronic states, and few-cycle pulses to cover multiple electronic transitions are highly desirable. Sample exposure may be reduced through acousto-optic shutters synchronized with digital delay generators, but it remains to be seen whether the advantages of high throughput could be carried over to 0.1–1 MHz repetition rates, which may be more relevant[132] for srMES, along with a broad bandwidth.

Shot-to-shot pulse phase and amplitude shaping techniques [Figs. 2(a) and 2(b)] rival those of frequency combs in terms of the equivalent number of mechanically moving parts, with even greater flexibility regarding amplitude shaping and the bandwidth. In this regard, any extension of AOPDF-based shot-to-shot shaping [Fig. 2(b)] to collect aMES spectra at higher repetition rates, somewhat akin to the 100 kHz shot-to-shot implementation of hMES [Fig. 5(d)], offers a proportional throughput increase combined with a robust approach capable of both hMES and aMES measurements using a single-beam geometry. Although commercial AOPDFs that operate at repetition rates higher than 1 kHz are available, this may come at the cost of increased constraints regarding the shaping bandwidth and delay scan range. Equivalently, extensions of the 100 kHz shot-to-shot shaping approach to aMES, possibly using two SLM based pulse shapers, can offer benefits of higher detection sensitivity not limited by the line camera CCD. With improvements in line readout rates, this approach is, in principle, scalable to repetition rates higher than 100 kHz but again limited by constraints regarding line camera detection sensitivity and the acoustic mask.

In this context, recent extensions of the AOPM approach to srMES to demonstrate rapid delay scanning[65] [Fig. 3(f)] are quite relevant. As mentioned in Sec. II D, the AOPM approach offers *dynamic* phase cycling, which is independent of the repetition rate or acoustic mask update rate. Combining this feature with rapid delay scanning offers the ability to collect dynamically phase-cycled srMES 2D spectra within a few seconds. In the cases where continuous delay scanning is not possible, sparse delay sampling[133,134] algorithms could be implemented to effectively reconstruct the 2D signal with data compression exceeding more than 75%, therefore minimizing continuous sample exposure to the laser.

Even though fully collinear aMES was already introduced in 2003 by Warren and co-workers, spatially resolved measurements based on a diffraction-limited illumination spot have only been a very recent development. Perhaps this suggests that the need for spatial resolution is scientifically motivated by emerging questions. For instance, in the community of organic photovoltaics, it is well known that the device performance correlates with thin-film nanomorphology.[4] Often, high-boiling point solvent additives and annealing conditions are tweaked to achieve optimal device photocurrent efficiencies. Similar effects are also known in the case of perovskite-based photovoltaics where exciton diffusion rates were reported[12] to be morphology dependent and pump–probe microscopy signals were reported to change sign[135] at grain boundaries. There is a need for a fundamental understanding of how nanomorphology affects ultrafast exciton delocalization and charge-transfer dynamics, which is where srMES can be instrumental in providing a fresh perspective to the community. In a slightly different context of photosynthetic energy and charge transfer, it is now well known[1] that ensemble dephasing across several proteins obscures the dephasing timescales of coherent vibrational–electronic wavepackets between one-quantum electronic states. Knowing such timescales is of relevance not only for a refined theoretical understanding but also for possible applications of similar design principles in artificial light-harvesting systems.[136] In the future, sub-ensemble measurements to identify the "ensemble dephasing-free" timescales of quantum decoherence between excited electronic states can be made possible by combinations of higher detection sensitivity and beyond diffraction-limited spatial resolution. Perhaps the sensitivity of aMES to exciton–exciton annihilation could also be leveraged to perform spatially offset[137] excitation and directly track exciton diffusion within photosynthetic membranes.

ACKNOWLEDGMENTS

V.T. thanks Dr. Rohan Singh for helpful discussions regarding optical frequency combs. V.T. acknowledges support from the Department of Atomic Energy, India, Grant Sanction No. 58/20/31/2019-BRNS, and the Science and Engineering Research Board, India, under Grant Sanction Nos. CRG/2019/003691 and IPA/2020/000033. V.T. also acknowledges support from the Infosys Foundation, Bangalore.

DATA AVAILABILITY

Data sharing is not applicable to this article as no new data were created or analyzed in this study.

REFERENCES

[1] D. M. Jonas, "Vibrational and nonadiabatic coherence in 2D electronic spectroscopy, the Jahn–Teller effect, and energy transfer," Annu. Rev. Phys. Chem. **69**, 327–352 (2018).
[2] W. Domcke, D. R. Yarkony, and H. Köppel, *Conical Intersections* (World Scientific, 2011).
[3] P. J. M. Johnson, A. Halpin, T. Morizumi, V. I. Prokhorenko, O. P. Ernst, and R. J. D. Miller, "Local vibrational coherences drive the primary photochemistry of vision," Nat. Chem. **7**, 980–986 (2015).

[4]A. A. Mohapatra, V. Tiwari, and S. Patil, "Energy transfer in ternary blend organic solar cells: Recent insights and future directions," Energy Environ. Sci. **14**, 302–319 (2021).
[5]J. Cao *et al.*, "Quantum biology revisited," Sci. Adv. **6**, eaaz4888 (2020).
[6]W. P. Aue, E. Bartholdi, and R. R. Ernst, "Two-dimensional spectroscopy. Application to nuclear magnetic resonance," J. Chem. Phys. **64**, 2229–2246 (1976).
[7]D. M. Jonas, "Optical analogs of 2D NMR," Science **300**, 1515–1517 (2003).
[8]D. M. Jonas, "Two-dimensional femtosecond spectroscopy," Annu. Rev. Phys. Chem. **54**, 425–463 (2003).
[9]H. Wu and M. A. Berg, "Multiple population-period transient spectroscopy (MUPPETS) in excitonic systems," J. Chem. Phys. **138**, 034201 (2013).
[10]S. Savikhin, D. R. Buck, and W. S. Struve, "Oscillating anisotropies in a bacteriochlorophyll protein: Evidence for quantum beating between exciton levels," Chem. Phys. **223**, 303–312 (1997).
[11]A. C. Jones, N. M. Kearns, J.-J. Ho, J. T. Flach, and M. T. Zanni, "Impact of non-equilibrium molecular packings on singlet fission in microcrystals observed using 2D white-light microscopy," Nat. Chem. **12**, 40–47 (2020).
[12]Z. Guo, J. S. Manser, Y. Wan, P. V. Kamat, and L. Huang, "Spatial and temporal imaging of long-range charge transport in perovskite thin films by ultrafast microscopy," Nat. Commun. **6**, 7471–7478 (2015).
[13]F. D. Fuller and J. P. Ogilvie, "Experimental implementations of two-dimensional fourier transform electronic spectroscopy," Annu. Rev. Phys. Chem. **66**, 667–690 (2015).
[14]K. A. Nelson, R. Casalegno, R. J. D. Miller, and M. D. Fayer, "Laser-induced excited state and ultrasonic wave gratings: Amplitude and phase grating contributions to diffraction," J. Chem. Phys. **77**, 1144–1152 (1982).
[15]A. M. Weiner, "Ultrafast optical pulse shaping: A tutorial review," Opt. Commun. **284**, 3669–3692 (2011), part of Special Issue: Optical Pulse Shaping, Arbitrary Waveform Generation, and Pulse Characterization.
[16]J. Tull, M. Dugan, and W. Warren, "High-resolution, ultrafast laser pulse shaping and its applications," in *Advances in Magnetic and Optical Resonance*, edited by W. S. Warren (Academic Press, 1997), Vol. 20, pp. I–II.
[17]P. F. Tekavec, T. R. Dyke, and A. H. Marcus, "Wave packet interferometry and quantum state reconstruction by acousto-optic phase modulation," J. Chem. Phys. **125**, 194303 (2006).
[18]P. F. Tekavec, G. A. Lott, and A. H. Marcus, "Fluorescence-detected two-dimensional electronic coherence spectroscopy by acousto-optic phase modulation," J. Chem. Phys. **127**, 214307 (2007).
[19]C. R. Baiz, D. Schach, and A. Tokmakoff, "Ultrafast 2D IR microscopy," Opt. Express **22**, 18724–18735 (2014).
[20]K. J. Karki, J. Chen, A. Sakurai, Q. Shi, A. T. Gardiner, O. Kühn, R. J. Cogdell, and T. Pullerits, "Before Förster. Initial excitation in photosynthetic light harvesting," Chem. Sci. **10**, 7923–7928 (2019).
[21]B. Brüggemann, P. Kjellberg, and T. Pullerits, "Non-perturbative calculation of 2D spectra in heterogeneous systems: Exciton relaxation in the FMO complex," Chem. Phys. Lett. **444**, 192–196 (2007).
[22]D. A. Blank, L. J. Kaufman, and G. R. Fleming, "Fifth-order two-dimensional Raman spectra of CS_2 are dominated by third-order cascades," J. Chem. Phys. **111**, 3105–3114 (1999).
[23]Z. Zhang, K. L. Wells, M. T. Seidel, and H.-S. Tan, "Fifth-order three-dimensional electronic spectroscopy using a pump–probe configuration," J. Phys. Chem. B **117**, 15369–15385 (2013).
[24]A. D. Bristow, D. Karaiskaj, X. Dai, and S. T. Cundiff, "All-optical retrieval of the global phase for two-dimensional Fourier-transform spectroscopy," Opt. Express **16**, 18017–18027 (2008).
[25]S. M. Gallagher Faeder and D. M. Jonas, "Two-dimensional electronic correlation and relaxation spectra: Theory and model calculations," J. Phys. Chem. A **103**, 10489–10505 (1999).
[26]J. A. Myers, K. L. M. Lewis, P. F. Tekavec, and J. P. Ogilvie, "Two-color two-dimensional Fourier transform electronic spectroscopy with a pulse-shaper," Opt. Express **16**, 17420–17428 (2008).
[27]A. J. Musser, M. Liebel, C. Schnedermann, T. Wende, T. B. Kehoe, A. Rao, and P. Kukura, "Evidence for conical intersection dynamics mediating ultrafast singlet exciton fission," Nat. Phys. **11**, 352–357 (2015).
[28]C. Schnedermann, J. Sung, R. Pandya, S. D. Verma, R. Y. S. Chen, N. Gauriot, H. M. Bretscher, P. Kukura, and A. Rao, "Ultrafast tracking of exciton and charge carrier transport in optoelectronic materials on the nanometer scale," J. Phys. Chem. Lett. **10**, 6727–6733 (2019).
[29]J. Jiang, W. S. Warren, and M. C. Fischer, "Crossed-beam pump-probe microscopy," Opt. Express **28**, 11259–11266 (2020).
[30]A. D. Bristow, D. Karaiskaj, X. Dai, T. Zhang, C. Carlsson, K. R. Hagen, R. Jimenez, and S. T. Cundiff, "A versatile ultrastable platform for optical multidimensional Fourier-transform spectroscopy," Rev. Sci. Instrum. **80**, 073108 (2009).
[31]M. L. Cowan, J. P. Ogilvie, and R. J. D. Miller, "Two-dimensional spectroscopy using diffractive optics based phased-locked photon echoes," Chem. Phys. Lett. **386**, 184–189 (2004).
[32]U. Selig, F. Langhojer, F. Dimler, T. Löhrig, C. Schwarz, B. Gieseking, and T. Brixner, "Inherently phase-stable coherent two-dimensional spectroscopy using only conventional optics," Opt. Lett. **33**, 2851–2853 (2008).
[33]A. P. Spencer and L. X. Chen, "Rapid acquisition of broadband two-dimensional electronic spectra by continuous scanning with conventional delay lines," Opt. Lett. **45**, 2942–2945 (2020).
[34]E. Harel, A. F. Fidler, and G. S. Engel, "Real-time mapping of electronic structure with single-shot two-dimensional electronic spectroscopy," Proc. Natl. Acad. Sci. U. S. A. **107**, 16444–16447 (2010).
[35]W. Wagner, C. Li, J. Semmlow, and W. S. Warren, "Rapid phase-cycled two-dimensional optical spectroscopy in fluorescence and transmission mode," Opt. Express **13**, 3697–3706 (2005).
[36]J. C. Vaughan, T. Hornung, K. W. Stone, and K. A. Nelson, "Coherently controlled ultrafast four-wave mixing spectroscopy," J. Phys. Chem. A **111**, 4873–4883 (2007).
[37]E. M. Grumstrup, S.-H. Shim, M. A. Montgomery, N. H. Damrauer, and M. T. Zanni, "Facile collection of two-dimensional electronic spectra using femtosecond pulse-shaping technology," Opt. Express **15**, 16681–16689 (2007).
[38]P. Tournois, "Acousto-optic programmable dispersive filter for adaptive compensation of group delay time dispersion in laser systems," Opt. Commun. **140**, 245–249 (1997).
[39]B. Lomsadze and S. T. Cundiff, "Frequency combs enable rapid and high-resolution multidimensional coherent spectroscopy," Science **357**, 1389–1391 (2017).
[40]B. Lomsadze, B. C. Smith, and S. T. Cundiff, "Tri-comb spectroscopy," Nat. Photonics **12**, 676–680 (2018).
[41]S. Mueller, J. Lüttig, P. Malý, L. Ji, J. Han, M. Moos, T. B. Marder, U. H. F. Bunz, A. Dreuw, C. Lambert, and T. Brixner, "Rapid multiple-quantum three-dimensional fluorescence spectroscopy disentangles quantum pathways," Nat. Commun. **10**, 4735 (2019).
[42]A. M. Weiner, D. E. Leaird, J. S. Patel, and J. R. Wullert, "Programmable femtosecond pulse shaping by use of a multielement liquid-crystal phase modulator," Opt. Lett. **15**, 326–328 (1990).
[43]D. Goswami, "Optical pulse shaping approaches to coherent control," Phys. Rep. **374**, 385–481 (2003).
[44]D. Yelin, D. Meshulach, and Y. Silberberg, "Adaptive femtosecond pulse compression," Opt. Lett. **22**, 1793–1795 (1997).
[45]B. Xu, Y. Coello, V. V. Lozovoy, D. A. Harris, and M. Dantus, "Pulse shaping of octave spanning femtosecond laser pulses," Opt. Express **14**, 10939–10944 (2006).
[46]M. M. Wefers and K. A. Nelson, "Generation of high-fidelity programmable ultrafast optical waveforms," Opt. Lett. **20**, 1047–1049 (1995).
[47]H.-S. Tan, "Theory and phase-cycling scheme selection principles of collinear phase coherent multi-dimensional optical spectroscopy," J. Chem. Phys. **129**, 124501 (2008).
[48]S. Goetz, D. Li, V. Kolb, J. Pflaum, and T. Brixner, "Coherent two-dimensional fluorescence micro-spectroscopy," Opt. Express **26**, 3915–3925 (2018).
[49]D. Keusters, H.-S. Tan, and W. S. Warren, Role of pulse phase and direction in two-dimensional optical spectroscopy," J. Phys. Chem. A **103**, 10369–10380 (1999).
[50]P. Tian, D. Keusters, Y. Suzaki, and W. S. Warren, "Femtosecond phase-coherent two-dimensional spectroscopy," Science **300**, 1553–1555 (2003).

[51] S.-H. Shim, D. B. Strasfeld, Y. L. Ling, and M. T. Zanni, "Automated 2D IR spectroscopy using a mid-IR pulse shaper and application of this technology to the human islet amyloid polypeptide," Proc. Natl. Acad. Sci. U. S. A. **104**, 14197–14202 (2007).
[52] J. S. Ostrander, A. L. Serrano, A. Ghosh, and M. T. Zanni, "Spatially resolved two-dimensional infrared spectroscopy via wide-field microscopy," ACS Photonics **3**, 1315–1323 (2016).
[53] B. M. Luther, K. M. Tracy, M. Gerrity, S. Brown, and A. T. Krummel, "2D IR spectroscopy at 100 kHz utilizing a Mid-IR OPCPA laser source," Opt. Express **24**, 4117–4127 (2016).
[54] N. M. Kearns, R. D. Mehlenbacher, A. C. Jones, and M. T. Zanni, "Broadband 2D electronic spectrometer using white light and pulse shaping: Noise and signal evaluation at 1 and 100 kHz," Opt. Express **25**, 7869–7883 (2017).
[55] A. C. Jones, N. M. Kearns, M. Bohlmann Kunz, J. T. Flach, and M. T. Zanni, "Multidimensional spectroscopy on the microscale: Development of a multimodal imaging system incorporating 2D white-light spectroscopy, broadband transient absorption, and atomic force microscopy," J. Phys. Chem. A **123**, 10824–10836 (2019).
[56] P. F. Tekavec, J. A. Myers, K. L. M. Lewis, and J. P. Ogilvie, "Two-dimensional electronic spectroscopy with a continuum probe," Opt. Lett. **34**, 1390–1392 (2009).
[57] N. Krebs, I. Pugliesi, J. Hauer, and E. Riedle, "Two-dimensional Fourier transform spectroscopy in the ultraviolet with sub-20 fs pump pulses and 250–720 nm supercontinuum probe," New J. Phys. **15**, 085016 (2013).
[58] M. Kullmann, S. Ruetzel, J. Buback, P. Nuernberger, and T. Brixner, "Reaction dynamics of a molecular switch unveiled by coherent two-dimensional electronic spectroscopy," J. Am. Chem. Soc. **133**, 13074–13080 (2011).
[59] Z. Zhang, K. L. Wells, E. W. J. Hyland, and H.-S. Tan, "Phase-cycling schemes for pump–probe beam geometry two-dimensional electronic spectroscopy," Chem. Phys. Lett. **550**, 156–161 (2012).
[60] Z. Zhang, K. L. Wells, and H.-S. Tan, "Purely absorptive fifth-order three-dimensional electronic spectroscopy," Opt. Lett. **37**, 5058–5060 (2012).
[61] P. Brosseau, S. Palato, H. Seiler, H. Baker, and P. Kambhampati, "Fifth-order two-quantum absorptive two-dimensional electronic spectroscopy of CdSe quantum dots," J. Chem. Phys. **153**, 234703 (2020).
[62] S. Draeger, S. Roeding, and T. Brixner, "Rapid-scan coherent 2D fluorescence spectroscopy," Opt. Express **25**, 3259–3267 (2017).
[63] M. K. Yetzbacher, T. L. Courtney, W. K. Peters, K. A. Kitney, E. R. Smith, and D. M. Jonas, "Spectral restoration for femtosecond spectral interferometry with attosecond accuracy," J. Opt. Soc. Am. B **27**, 1104–1117 (2010).
[64] J. Kim, J. Jeon, T. H. Yoon, and M. Cho, "Two-dimensional electronic spectroscopy of bacteriochlorophyll a with synchronized dual mode-locked lasers," Nat. Commun. **11**, 6029 (2020).
[65] T. M. Autry, G. Moody, J. Fraser, C. McDonald, R. P. Mirin, and K. Silverman, "Single-scan acquisition of multiple multidimensional spectra," Optica **6**, 735–744 (2019).
[66] E. W. Martin and S. T. Cundiff, "Inducing coherent quantum dot interactions," Phys. Rev. B **97**, 081301 (2018).
[67] J. Lavoie, T. Landes, A. Tamimi, B. J. Smith, A. H. Marcus, and M. G. Raymer, "Phase-modulated interferometry, spectroscopy, and refractometry using entangled photon pairs," Adv. Quantum Technol. **3**, 1900114 (2020).
[68] D. J. Jones, S. A. Diddams, J. K. Ranka, A. Stentz, R. S. Windeler, J. L. Hall, and S. T. Cundiff, "Carrier-envelope phase control of femtosecond mode-locked lasers and direct optical frequency synthesis," Science **288**, 635–640 (2000).
[69] W. S. Warren and A. H. Zewail, "Optical analogs of NMR phase coherent multiple pulse spectroscopy," J. Chem. Phys. **75**, 5956–5958 (1981).
[70] F. A. Damtie, A. Wacker, T. o. Pullerits, and K. J. Karki, "Two-dimensional action spectroscopy of excitonic systems: Explicit simulation using a phase-modulation technique," Phys. Rev. A **96**, 053830 (2017).
[71] N. F. Scherer, R. J. Carlson, A. Matro, M. Du, A. J. Ruggiero, V. Romero-Rochin, J. A. Cina, G. R. Fleming, and S. A. Rice, "Fluorescence-detected wave packet interferometry: Time resolved molecular spectroscopy with sequences of femtosecond phase-locked pulses," J. Chem. Phys. **95**, 1487–1511 (1991).
[72] G. A. Lott, A. Perdomo-Ortiz, J. K. Utterback, J. R. Widom, A. Aspuru-Guzik, and A. H. Marcus, "Conformation of self-assembled porphyrin dimers in liposome vesicles by phase-modulation 2D fluorescence spectroscopy," Proc. Natl. Acad. Sci. U. S. A. **108**, 16521–16526 (2011).
[73] A. Perdomo-Ortiz, J. R. Widom, G. A. Lott, A. Aspuru-Guzik, and A. H. Marcus, "Conformation and electronic population transfer in membrane-supported self-assembled porphyrin dimers by 2D fluorescence spectroscopy," J. Phys. Chem. B **116**, 10757–10770 (2012).
[74] J. R. Widom, W. Lee, A. Perdomo-Ortiz, D. Rappoport, T. F. Molinski, A. Aspuru-Guzik, and A. H. Marcus, "Temperature-dependent conformations of a membrane supported zinc porphyrin tweezer by 2D fluorescence spectroscopy," J. Phys. Chem. A **117**, 6171–6184 (2013).
[75] J. R. Widom, N. P. Johnson, P. H. von Hippel, and A. H. Marcus, "Solution conformation of 2-aminopurine dinucleotide determined by ultraviolet two-dimensional fluorescence spectroscopy," New J. Phys. **15**, 025028 (2013).
[76] V. Tiwari, Y. A. Matutes, A. Konar, Z. Yu, M. Ptaszek, D. F. Bocian, D. Holten, C. Kirmaier, and J. P. Ogilvie, "Strongly coupled bacteriochlorin dyad studied using phase-modulated fluorescence-detected two-dimensional electronic spectroscopy," Opt. Express **26**, 22327–22341 (2018).
[77] S. Mueller, J. Lüttig, L. Brenneis, D. Oron, and T. Brixner, "Observing multiexciton correlations in colloidal semiconductor quantum dots via multiple-quantum two-dimensional fluorescence spectroscopy," ACS Nano **15**, 4647 (2021).
[78] G. Nardin, T. M. Autry, K. L. Silverman, and S. T. Cundiff, "Multidimensional coherent photocurrent spectroscopy of a semiconductor nanostructure," Opt. Express **21**, 28617–28627 (2013).
[79] K. J. Karki, J. R. Widom, J. Seibt, I. Moody, M. C. Lonergan, T. Pullerits, and A. H. Marcus, "Coherent two-dimensional photocurrent spectroscopy in a PbS quantum dot photocell," Nat. Commun. **5**, 5869 (2014).
[80] A. J. Nozik, "Multiple exciton generation in semiconductor quantum dots," Chem. Phys. Lett. **457**, 3–11 (2008).
[81] B. Yang, J. Chen, Q. Shi, Z. Wang, M. Gerhard, A. Dobrovolsky, I. G. Scheblykin, K. J. Karki, K. Han, and T. Pullerits, "High resolution mapping of two-photon excited photocurrent in perovskite microplate photodetector," J. Phys. Chem. Lett. **9**, 5017–5022 (2018).
[82] E. Vella, H. Li, P. Grégoire, S. M. Tuladhar, M. S. Vezie, S. Few, C. M. Bazán, J. Nelson, C. Silva-Acuña, and E. R. Bittner, "Ultrafast decoherence dynamics govern photocarrier generation efficiencies in polymer solar cells," Sci. Rep. **6**, 29437 (2016).
[83] P. Grégoire, A. R. Srimath Kandada, E. Vella, C. Tao, R. Leonelli, and C. Silva, "Incoherent population mixing contributions to phase-modulation two-dimensional coherent excitation spectra," J. Chem. Phys. **147**, 114201 (2017).
[84] S. Mukamel, "Communication: The origin of many-particle signals in nonlinear optical spectroscopy of non-interacting particles," J. Chem. Phys. **145**, 041102 (2016).
[85] S. Mukamel, R. Oszwałdowski, and L. Yang, "A coherent nonlinear optical signal induced by electron correlations," J. Chem. Phys. **127**, 221105 (2007).
[86] P. Malý, J. Lüttig, S. Mueller, M. H. Schreck, C. Lambert, and T. Brixner, "Coherently and fluorescence-detected two-dimensional electronic spectroscopy: Direct comparison on squaraine dimers," Phys. Chem. Chem. Phys. **22**, 21222–21237 (2020).
[87] A. A. S. Kalaee, F. Damtie, and K. J. Karki, "Differentiation of true nonlinear and incoherent mixing of linear signals in action-detected 2D spectroscopy," J. Phys. Chem. A **123**, 4119–4124 (2019).
[88] P. Malý, S. Mueller, J. Lüttig, C. Lambert, and T. Brixner, "Signatures of exciton dynamics and interaction in coherently and fluorescence-detected four- and six-wave-mixing two-dimensional electronic spectroscopy," J. Chem. Phys. **153**, 144204 (2020).
[89] S. Mueller, S. Draeger, X. Ma, M. Hensen, T. Kenneweg, W. Pfeiffer, and T. Brixner, "Fluorescence-detected two-quantum and one-quantum–two-quantum 2D electronic spectroscopy," J. Phys. Chem. Lett. **9**, 1964–1969 (2018).
[90] J. Dostál, F. Fennel, F. Koch, S. Herbst, F. Würthner, and T. Brixner, "Direct observation of exciton–exciton interactions," Nat. Commun. **9**, 2466 (2018).
[91] T. Brixner, "Vibrational dynamics via multidimensional electronic spectroscopy," Asian J. Phys. **30**, 303–318 (2019).

[92]A. K. De, D. Monahan, J. M. Dawlaty, and G. R. Fleming, "Two-dimensional fluorescence-detected coherent spectroscopy with absolute phasing by confocal imaging of a dynamic grating and 27-step phase-cycling," J. Chem. Phys. **140**, 194201 (2014).
[93]S. Roeding and T. Brixner, "Coherent two-dimensional electronic mass spectrometry," Nat. Commun. **9**, 2519 (2018).
[94]L. Bruder, U. Bangert, M. Binz, D. Uhl, R. Vexiau, N. Bouloufa-Maafa, O. Dulieu, and F. Stienkemeier, "Coherent multidimensional spectroscopy of dilute gas-phase nanosystems," Nat. Commun. **9**, 4823 (2018).
[95]L. Whaley-Mayda, A. Guha, S. B. Penwell, and A. Tokmakoff, "Fluorescence-encoded infrared vibrational spectroscopy with single-molecule sensitivity," J. Am. Chem. Soc. **143**, 3060–3064 (2021).
[96]P. Malý and T. Mančal, "Signatures of exciton delocalization and exciton–exciton annihilation in fluorescence-detected two-dimensional coherent spectroscopy," J. Phys. Chem. Lett. **9**, 5654–5659 (2018).
[97]T. Kunsel, V. Tiwari, Y. A. Matutes, A. T. Gardiner, R. J. Cogdell, J. P. Ogilvie, and T. L. C. Jansen, "Simulating fluorescence-detected two-dimensional electronic spectroscopy of multichromophoric systems," J. Phys. Chem. B **123**, 394–406 (2019).
[98]W. J. D. Beenken, M. Dahlbom, P. Kjellberg, and T. Pullerits, "Potential surfaces and delocalization of excitons in dimers," J. Chem. Phys. **117**, 5810–5820 (2002).
[99]H. S. Kang, N. N. Esemoto, J. R. Diers, D. M. Niedzwiedzki, J. A. Greco, J. Akhigbe, Z. Yu, C. Pancholi, G. Viswanathan Bhagavathy, J. K. Nguyen, C. Kirmaier, R. R. Birge, M. Ptaszek, D. Holten, and D. F. Bocian, "Effects of strong electronic coupling in chlorin and bacteriochlorin dyads," J. Phys. Chem. A **120**, 379–395 (2016).
[100]O. Kühn, T. Mančal, and T. Pullerits, "Interpreting fluorescence detected two-dimensional electronic spectroscopy," J. Phys. Chem. Lett. **11**, 838–842 (2020).
[101]M. Aeschlimann, T. Brixner, A. Fischer, C. Kramer, P. Melchior, W. Pfeiffer, C. Schneider, C. Strüber, P. Tuchscherer, and D. V. Voronine, "Coherent two-dimensional nanoscopy," Science **333**, 1723–1726 (2011).
[102]B. Huber, S. Pres, E. Wittmann, L. Dietrich, J. Lüttig, D. Fersch, E. Krauss, D. Friedrich, J. Kern, V. Lisinetskii, M. Hensen, B. Hecht, R. Bratschitsch, E. Riedle, and T. Brixner, "Space- and time-resolved UV-to-NIR surface spectroscopy and 2D nanoscopy at 1 MHz repetition rate," Rev. Sci. Instrum. **90**, 113103 (2019).
[103]D. Li, E. Titov, M. Roedel, V. Kolb, S. Goetz, R. Mitric, J. Pflaum, and T. Brixner, "Correlating nanoscale optical coherence length and microscale topography in organic materials by coherent two-dimensional microspectroscopy," Nano Lett. **20**, 6452–6458 (2020).
[104]V. Tiwari, Y. A. Matutes, A. T. Gardiner, T. L. C. Jansen, R. J. Cogdell, and J. P. Ogilvie, "Spatially-resolved fluorescence-detected two-dimensional electronic spectroscopy probes varying excitonic structure in photosynthetic bacteria," Nat. Commun. **9**, 4219 (2018).
[105]Z. T. Armstrong, M. B. Kunz, A. C. Jones, and M. T. Zanni, "Thermal annealing of singlet fission microcrystals reveals the benefits of charge transfer couplings and slip-stacked packing," J. Phys. Chem. C **124**, 15123–15131 (2020).
[106]D. Li, C. Trovatello, S. Dal Conte, M. Nuß, G. Soavi, G. Wang, A. C. Ferrari, G. Cerullo, and T. Brixner, "Exciton-phonon coupling strength in single-layer $MoSe_2$ at room temperature," Nat. Commun. **12**, 954 (2021).
[107]V. Moulisová, L. Luer, S. Hoseinkhani, T. H. P. Brotosudarmo, A. M. Collins, G. Lanzani, R. E. Blankenship, and R. J. Cogdell, "Low light adaptation: Energy transfer processes in different types of light harvesting complexes from Rhodopseudomonas palustris," Biophys. J. **97**, 3019–3028 (2009).
[108]J. D. Hybl, A. W. Albrecht, S. M. G. Faeder, and D. M. Jonas, "Two-dimensional electronic spectroscopy," Chem. Phys. Lett. **297**, 307 (1998).
[109]W. E. Moerner and D. P. Fromm, "Methods of single-molecule fluorescence spectroscopy and microscopy," Rev. Sci. Instrum. **74**, 3597–3619 (2003).
[110]J. P. Camden, J. A. Dieringer, J. Zhao, and R. P. Van Duyne, "Controlled plasmonic nanostructures for surface-enhanced spectroscopy and sensing," Acc. Chem. Res. **41**, 1653–1661 (2008).
[111]S. Nie and S. R. Emory, "Probing single molecules and single nanoparticles by surface-enhanced Raman scattering," Science **275**, 1102–1106 (1997).
[112]S. Yampolsky, D. A. Fishman, S. Dey, E. Hulkko, M. Banik, E. O. Potma, and V. A. Apkarian, "Seeing a single molecule vibrate through time-resolved coherent anti-Stokes Raman scattering," Nat. Photonics **8**, 650–656 (2014).
[113]J. P. Kraack and P. Hamm, "Vibrational ladder-climbing in surface-enhanced, ultrafast infrared spectroscopy," Phys. Chem. Chem. Phys. **18**, 16088–16093 (2016).
[114]M. K. Petti, J. S. Ostrander, V. Saraswat, E. R. Birdsall, K. L. Rich, J. P. Lomont, M. S. Arnold, and M. T. Zanni, "Enhancing the signal strength of surface sensitive 2D IR spectroscopy," J. Chem. Phys. **150**, 024707 (2019).
[115]R. T. Mackin, B. Cohn, A. Gandman, J. D. Leger, L. Chuntonov, and I. V. Rubtsov, "Surface-enhanced dual-frequency two-dimensional vibrational spectroscopy of thin layers at an interface," J. Phys. Chem. C **122**, 11015–11023 (2018).
[116]A. Gandman, R. Mackin, B. Cohn, I. V. Rubtsov, and L. Chuntonov, "Two-dimensional fano lineshapes in ultrafast vibrational spectroscopy of thin molecular layers on plasmonic arrays," J. Phys. Chem. Lett. **8**, 3341–3346 (2017).
[117]R. Bardhan, N. K. Grady, and N. J. Halas, "Nanoscale control of near-infrared fluorescence enhancement using Au nanoshells," Small **4**, 1716–1722 (2008).
[118]R. F. Aroca, G. Y. Teo, H. Mohan, A. R. Guerrero, P. Albella, and F. Moreno, "Plasmon-enhanced fluorescence and spectral modification in SHINEF," J. Phys. Chem. C **115**, 20419–20424 (2011).
[119]E. Wientjes, J. Renger, A. G. Curto, R. Cogdell, and N. F. van Hulst, "Strong antenna-enhanced fluorescence of a single light-harvesting complex shows photon antibunching," Nat. Commun. **5**, 4236 (2014).
[120]E. C. Le Ru, P. G. Etchegoin, J. Grand, N. Félidj, J. Aubard, and G. Lévi, "Mechanisms of spectral profile modification in surface-enhanced fluorescence," J. Phys. Chem. C **111**, 16076–16079 (2007).
[121]H. Blom and J. Widengren, "Stimulated emission depletion microscopy," Chem. Rev. **117**, 7377–7427 (2017).
[122]B. Hecht, B. Sick, U. P. Wild, V. Deckert, R. Zenobi, O. J. F. Martin, and D. W. Pohl, "Scanning near-field optical microscopy with aperture probes: Fundamentals and applications," J. Chem. Phys. **112**, 7761–7774 (2000).
[123]A. Kinkhabwala, Z. Yu, S. Fan, Y. Avlasevich, K. Müllen, and W. E. Moerner, "Large single-molecule fluorescence enhancements produced by a bowtie nanoantenna," Nat. Photonics **3**, 654–657 (2009).
[124]M. J. Feldstein, P. Vöhringer, W. Wang, and N. F. Scherer, "Femtosecond optical spectroscopy and scanning probe microscopy," J. Phys. Chem. **100**, 4739–4748 (1996).
[125]C. C. Neacsu, S. Berweger, R. L. Olmon, L. V. Saraf, C. Ropers, and M. B. Raschke, "Near-field localization in plasmonic superfocusing: A nanoemitter on a tip," Nano Lett. **10**, 592–596 (2010).
[126]T. Umakoshi, M. Tanaka, Y. Saito, and P. Verma, "White nanolight source for optical nanoimaging," Sci. Adv. **6**, eaba4179 (2020).
[127]K. Taguchi, T. Umakoshi, S. Inoue, and P. Verma, "Broadband plasmon nanofocusing: Comprehensive study of broadband nanoscale light source," J. Phys. Chem. C **125**, 6378–6386 (2021).
[128]E. Verhagen, M. Spasenović, A. Polman, and L. K. Kuipers, "Nanowire plasmon excitation by adiabatic mode transformation," Phys. Rev. Lett. **102**, 203904 (2009).
[129]S. Berweger, J. M. Atkin, X. G. Xu, R. L. Olmon, and M. B. Raschke, "Femtosecond nanofocusing with full optical waveform control," Nano Lett. **11**, 4309–4313 (2011).
[130]V. Karvtsov, R. Ulbricht, J. M. Atkin, and M. B. Raschke, "Plasmonic nanofocused four-wave mixing for femtosecond near-field imaging," Nat. Nanotechnol. **11**, 459–464 (2016).
[131]S. Kim, N. Yu, X. Ma, Y. Zhu, Q. Liu, M. Liu, and R. Yan, "High external-efficiency nanofocusing for lens-free near-field optical nanoscopy," Nat. Photonics **13**, 636–643 (2019).
[132]G. Donnert, C. Eggeling, and S. W. Hell, "Major signal increase in fluorescence microscopy through dark-state relaxation," Nat. Methods **4**, 81–86 (2007).
[133]Z. Wang, S. Lei, K. J. Karki, A. Jakobsson, and T. Pullerits, "Compressed sensing for reconstructing coherent multidimensional spectra," J. Phys. Chem. A **124**, 1861–1866 (2020).

[134]I. Bhattacharya, J. J. Humston, C. M. Cheatum, and M. Jacob, "Accelerating two-dimensional infrared spectroscopy while preserving lineshapes using GIRAF," Opt. Lett. **42**, 4573–4576 (2017).
[135]C. Schnedermann, J. M. Lim, T. Wende, A. S. Duarte, L. Ni, Q. Gu, A. Sadhanala, A. Rao, and P. Kukura, "Sub-10 fs time-resolved vibronic optical microscopy," J. Phys. Chem. Lett. **7**, 4854–4859 (2016).
[136]G. D. Scholes *et al.*, "Using coherence to enhance function in chemical and biophysical systems," Nature **543**, 647 (2017).
[137]S. Y. Kwang and R. R. Frontiera, "Spatially offset femtosecond stimulated Raman spectroscopy: Observing exciton transport through a vibrational lens," J. Phys. Chem. Lett. **11**, 4337–4344 (2020).